Unitat de Química Física
Departament de Química
Universitat Autònoma de Barcelona

Els sotasignants Dr. Vicenç Branchadell i Gallo i Dra. Mariona Sodupe i Roure

Certifiquem

Que Xavier Solans Monfort ha realitzat sota la nostra direcció al Departament de Quimica de la universitat Autònoma de Barcelona el treball que porta per títol

Modelling of adsorption and catalytic processes in H^+ and Cu^+ exchanged ZSM-5 and CHA zeolites

que es presenta en aquesta memòria per optar el grau de doctor en Química.

Vicenç Branchadell i Gallo

Mariona Sodupe i Roure

Bellaterra, Setembre 2003

Als meus amics, als pares i a en Pau

Agraïments

M’agradaria escriure unes quantes línies per agrair a tots aquells que m’han ajudat molt en la realització d’aquesta tesi. Per no ser etern m’he centrat en l’entorn laboral, la resta ja ho sabeu de sempre.

Per començar, moltes gràcies! Mariona i Vicenç per la direcció que heu fet de la meva tesi. Estic molt satisfet de la vostra ajuda en mil i una coses, de la enorme quantitat de coses que m’heu ensenyat i també pel vostre gran tracte humà.

Així mateix, voldria agrair-li a en Joan Bertran la il·lusió per la ciència que m’ha transmès i els seus consells en les decisions importants.

També agrair a tots els companys de despatx que he tingut al llarg de la meva tesi. Gràcies per la vostra paciència en ensenyar-me, aguantar els meus crits i nervis, sobretot ara el final. Sobretot, però, gràcies per haver aconseguit, durant tants anys un molt bon ambient en el laboratori, que no voldria definir només com de treball, perquè crec que hi he deixat bons amics. En especial voldria destinar una línia per agrair al Luis que va ser qui em va patir més els primers dies.

No voldria deixar-me la resta de membres de la Unitat de Química Física, ja que estic molt content del bon ambient del que he gaudit amb tothom. Estaria bé que les futures generacions es poguessin sentir tan agraïdes del bon rotllo que han tingut en la Unitat.

Voldria també mencionar a la Generalitat de Catalunya i la Universitat Autònoma de Barcelona pel finançament que m’ha permès mantenir-me (no sense penúries) durant els 5 anys d’ elaboració de la tesis.

No quisiera olvidarme de todos aquellos que nos perdimos un mes en Castellón durante el Curso Interuniversitario de Química Teórica y Computacional. Allí descubrí que había más “locos” haciendo cálculos.

I want also to acknowledge to Joachim Sauer, all the staff of the Quantenchemie group in the Humboldt University and its visitors. Thank you for giving me the chance to visit your laboratory. I have learnt a lot from you and I will always remember my stay in Berlin.

Vorrei ringraziare inoltre il gruppo di Chimica Teorica e il gruppo di A. Zecchina dell'Università Degli Studi di Torino e in particolare il gruppo di Piero Ugliengo per la buona accoglienza che ho ricevuto, per tutto quello che ho imparato e per le amicizie che ho stretto. Sono in debito per la borsa Marie Curie Training che mi ha permesso di restare a Torino tre mesi in più.

Finalment, m'agradaria ressaltar la ajuda que he tingut des de petit de la meva família. Sense ells segurament aquesta tesis no hagués estat possible.

Contents

1. Introduction

The present thesis studies several processes that take place inside acidic or copper exchanged zeolites from a theoretical point of view. Two zeolites have been chosen: ZSM-5 and Chabazite. The thesis is divided in 7 chapters. The first one presents a general introduction to zeolites: their composition, structure, properties and uses, while the second one focuses on how these materials can be modelled, and which approaches are most the commonly used. The subsequent chapters describe the four different studies included in the present thesis. Each chapter will present a specific introduction to the problem, the goals of the study, a discussion of the obtained results and finally the concluding remarks. Chapters 3 and 4 are related with copper exchanged zeolites, chapter 3 describes the study of the catalytic decomposition of NO by Cu exchanged ZSM-5 (CuZSM-5) and chapter 4 reports the work done on the adsorption of molecular hydrogen in Cu exchanged Chabazite (CuCHA). The last two chapters refer to acidic zeolites. Chapter 5 presents the study of the keto-enol isomerization of acetaldehyde in proton exchanged ZSM-5 (HZSM-5) while chapter 6 describes the NH_3 adsorption on acidic Chabazite (HCHA).

1.1 General introduction to Zeolites

Zeolites are natural or synthesized aluminosilicate microporous solids that present a three-dimensional crystalline framework made of corner-sharing TO_4 tetrahedra, where T stands for Si or Al.[1-5] The name "zeolite" is Greek in origin. It comes from the words 'zein' (ζειν) and 'lithos' (λιθοσ) that mean boiling stone.[1,2] This name was first used in 1756 by the Swedish mineralogist Cronstedt, who discovered a new mineral that seemed to boil when heated because of the fast water loss.[6]

Zeolites are low-density materials and present channels and cavities in their three-dimensional framework. Each AlO_4 tetrahedra introduce a negative charge which is compensated by mono or divalent cations within the cavities. The general formula of zeolites is given by:

$$M_{m/Z}^{Z+}\left[Si_nAl_mO_{2(n+m)}\right]^{m-} \bullet qH_2O \qquad (1.1)$$

where M^{Z+} are extraframework cations (e.g. H^+, Na^+, K^+, Ca^{2+}, Mg^{2+}, Cu^+ or Cu^{2+} etc.) and qH_2O indicates extra-lattice water molecules. These molecules are easily removed by heating up to about 350 ºC.[7] This process is known as activation of the zeolite.

Zeolites can be divided in two groups: zeolites that have been found in nature and those that have been synthesized.[1] Natural zeolites are traditionally referred using long names such as Chabazite, Faujasite, or Mordenite. They are commonly found with alkali or alkali-earth metals as countercations and they are produced following two different routes:[1] one at low temperatures, associated with sedimentary processes and another one at high temperatures, linked to volcanic and thermal processes. Although they have been known for almost 250 years[8], it was not until researchers succeeded in producing synthetic zeolites[9] that they started to be widely used. Nowadays, all natural zeolite frameworks as well as a great variety of new ones can be synthesized. Synthetic zeolites avoid the problem of impurities, changes in chemical composition depending on the source and allow the control of their properties. Synthetic zeolites often have an acronym as a name, some examples are Zeolite A, X and Y or ZSM-5. The IUPAC has suggested a general way to name zeolite frameworks.[10] These names are formed by three capital letters, which correspond to the abbreviation of the natural name in those cases where a natural zeolite with the same framework exists. Thus, CHA stands for all the structures that have a Chabazite framework or FAU stands for all structures with a Faujasite framework. This latter case includes Faujasite, zeolite Y, zeolite X, and others.[10] That is, they have the same framework but they differ in their origin or in the aluminium content. Synthetic frameworks present three capital letters, which are generally related with the company that has synthesized them and the corresponding number or letter. Thus ZSM-5, ZSM-11, which are synthesized by Mobil Company, are called MFI (Mobil FIve) and MEL (Mobil ELeven), while those synthesized by Linde are called LT indicating Linde Type (LTL, LTA,...).

1.1.1 Structure

Zeolites are formed by the linking of TO_4 tetrahedra, which are the primary building units.[8] The union of several tetrahedra form what is known as the secondary building units (SBU).[1,2,5,7,10] These units are simple arrangements of tetrahedra that form

four-, six- or eight-membered rings or a combination of them. The expansion of these units in the three space directions generates the zeolite framework. The number of SBU is limited and the advantage of using these subunits is that one can identify several zeolite families constructed from the same SBU.[1,2] The unit cells of zeolites are specific for each zeolite type. As examples, Figure 1.1 and Figure 1.2 present the secondary building units and whole frameworks of Chabazite and ZSM-5, respectively, the two zeolites considered in the present thesis.

Chabazite's secondary building unit is formed by two parallel 6-membered rings connected through six 4-membered rings (Figure 1.1a).[11] The union of these SBU through three alternate vertices of each 6-membered ring creates two different channel systems: the 6-membered ring of the SBU and an 8-membered ring formed by the connection of 4 SBU (Figure 1.1b). The intersection of these channel systems, generates big elliptical cages. Each elliptical cage is connected to six neighbour cages through the 8-membered channels (Figure 1.1c). This natural zeolite is formed in volcanic rocks or in and around hot springs as a precipitate.[11,12]

ZSM-5 presents two different crystal phases depending on the temperature and each phase presents a different SBU.[13-15] At low temperatures ZSM-5 crystallizes in a monoclinic system with a secondary building unit formed by 24 tetrahedra, while at high temperatures it presents an orthorhombic lattice with a secondary building unit of 12 tetrahedra. The phase transition takes place around 340 K. The SBU related with the orthorhombic lattice is presented in Figure 1.2a. The arrangement of this subunit in one dimension generates sinusoidal chains (Figure 1.2b). Repeating this chain in one plane produces a 10-membered ring and finally the superposition of planes generates the three dimensional structure which is characterised by two channel systems, one straight and another one sinusoidal (Figure 1.2d). This zeolite was first synthesized by the Mobil Company in 1972.[16]

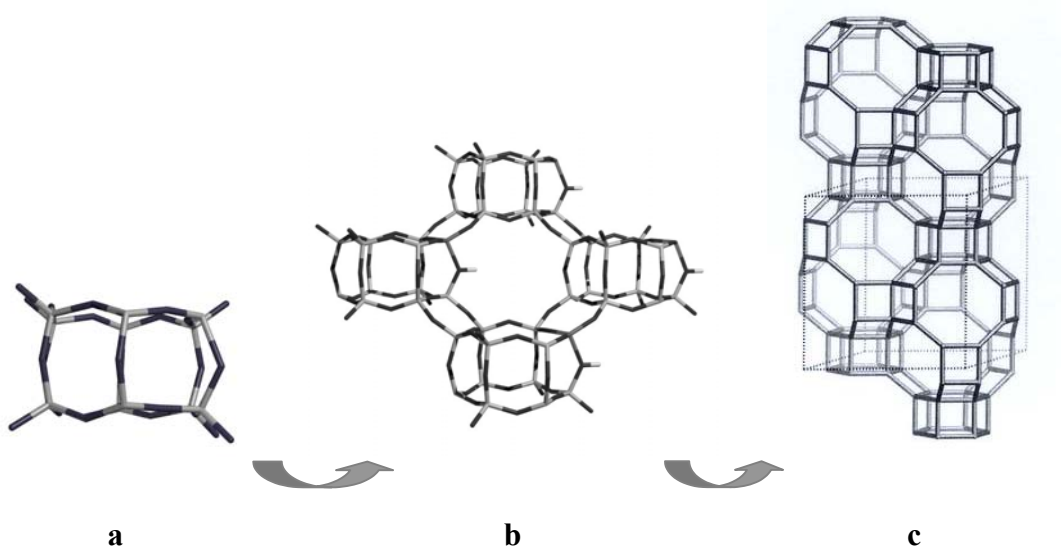

Figure 1.1 SBU of Chabazite and schematic representation of the construction of Chabazite framework.[10]

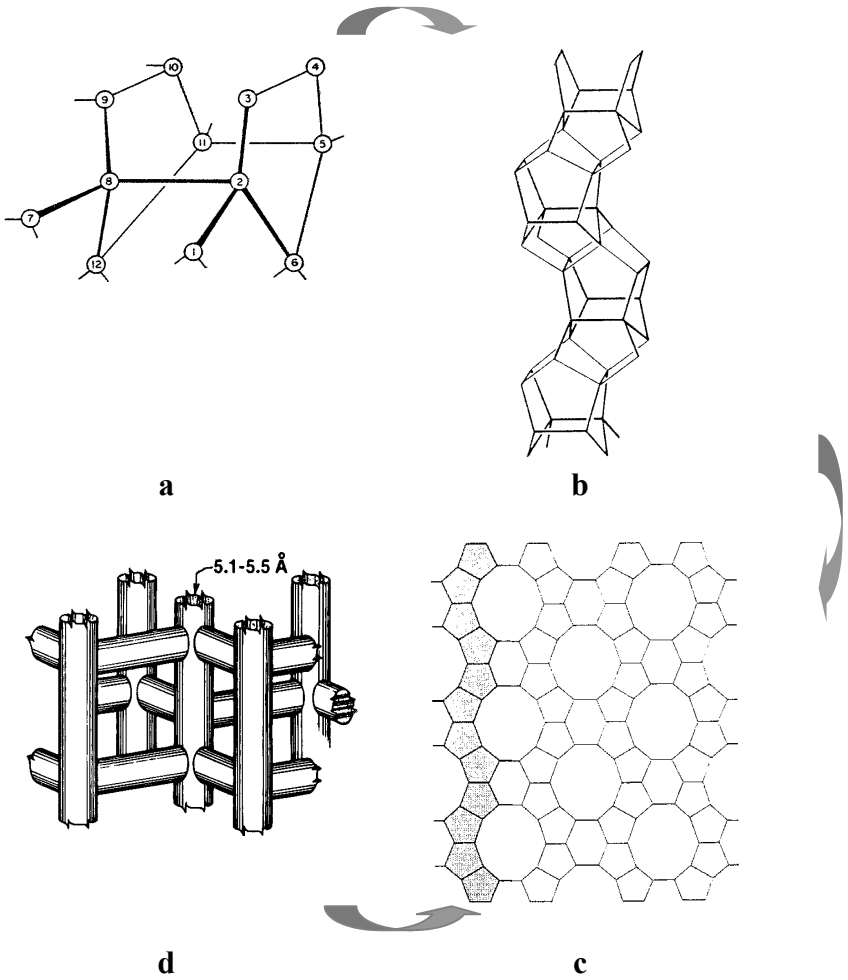

Figure 1.2 SBU of ZSM-5 and schematic representation of the construction of ZSM-5 framework.[13,14]

Zeolites are normally synthesized by mixing silica and aluminium gels, obtained from a great variety of sources, in OH^- or F^- solutions.[1] However, the final framework is highly influenced by the presence of organic molecules, called templates, as precursors of the channels.[2,9,17] These templates must be soluble in water and generate strong interactions with the Si-O bonds. In addition, they must be quite hydrophobic, not flexible and big. Typical templates are ammonium tetrasubstituted amines with a C/N ratio of 11-15. These substituents are the main responsible of the shape and size of the channels and also of the number of different channel systems. To generate channels, the substituents must be large enough to avoid the formation of isolated cavities. Channels are generated by the formation of the aluminosilicate around these molecules, which can be eliminated by heating after the zeolite synthesis. Synthetic methods are so elaborated that it is possible to control many variables during the zeolite formation such as the size and organization of the channels, or the Si/Al ratio.[17]

Zeolites can be classified according to several criteria. To start with, they are classified by the channel size[4,18] as: small, if the channel ring presents 8 or less tetrahedra, medium (if the number of tetrahedra lies between 10 and 8), large (up to 12) and ultra large (if more than 12 tetrahedra constitute the channel ring). Chabazite biggest channels present 8-membered rings, so that it belongs to the group of zeolites with small channels. In contrast, ZSM-5 presents two channel systems formed by 10-membered rings and thus belongs to the group of zeolites with medium pores.

A second criterion refers to the channel system dimensionality.[8,10] Zeolites are classified as one, two or three-dimensional systems. Both Chabazite and ZSM-5 present three-dimensional channel systems (see figures 1.1 and 1.2).

The Si/Al ratio is a fundamental characteristic of zeolites.[2,4,18] This Si/Al ratio is variable even in each zeolite type. However, each framework has a Si/Al range within which it is stable.[5] For example, for ZSM-5 this interval lies between 10 and ∞;[8] that is, up to pure silicon ZSM-5 (known as Silicalite). Normally, natural zeolites (as Chabazite) present lower Si/Al ratios than synthetic ones,[5] Mordenite being the most siliceous natural zeolite.[5] The distribution of Al substitution is controlled by the Loewenstein rule,[19] which states that pairs of neighbour AlO_4^- tetrahedra are forbidden. Thus, the lowest possible Si/Al ratio is 1, which has been obtained in zeolite-A. The active catalytic sites are normally located near aluminium but they are not easy to localize and

characterize, due to the lack of periodicity. Thus, they are normally analysed indirectly by their properties.

1.1.2 Properties and uses of zeolites

As mentioned, the substitution of one silicon per one aluminium atom (Si/Al substitution) introduces a negative charge that is normally compensated either by a proton or a metal cation. These compensating cations are the main responsible of most of the zeolite properties. These cations are easily exchanged in solution by controlling the conditions of the exchange process.[1,2,8] It is said that zeolites with high Si/Al ratio prefer larger cations than rich aluminium zeolites which present high selectivity for polyvalent cations.

Proton exchanged zeolites are mainly produced by the thermal elimination of ammonia from ammonium-exchanged zeolites. That is:

$$NH_4^+Z^- \xrightarrow{\Delta} H^+Z^- + NH_3 \qquad (1.2)$$

where Z^- stands for $\left[Si_nAl_mO_{2(n+m)}\right]^{m-}$

Proton exchanged zeolites present high acidity, which is attributed both to Brønsted and Lewis acid sites. Several authors have suggested that the zeolite acidity is similar to that of a solution of 70-75% of H_2SO_4.[20] Brønsted acid sites are thought to be formed by the protonation of one of the bridging oxygen atoms between the aluminium and the neighbour silicon tetrahedra, as it is shown in Figure 1.3. Lewis acidity is thought to be related with defects in the zeolite structure such as tricordinated aluminium or extraframework aluminium.[20]

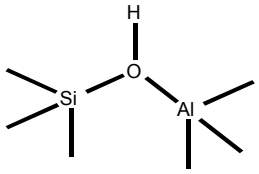

Figure 1.3 Brønsted acid site in zeolites

Zeolite acidity can be modified.[4,8,20] Within a determined zeolite framework, a change in the Si/Al ratio alters the acidity of the zeolite: the more aluminium is present, the greater is the number of acid sites. However, higher aluminium content also decreases the strength of the acidic existing sites. Moreover, the exchange of some protons by metal cations also affects the zeolite acidity, the more electropositive being the cation, the less acidic becoming the zeolite. Furthermore, one can also modify the acidity of the zeolite by the substitution of Al by B, Fe, Ga, etc.

On the other hand, several metal exchanged zeolites present interesting properties associated to the metal cation, the most remarkable ones involving transition metal cations such as Cu^{+}, Cu^{2+}, Fe^{2+}, Fe^{3+}, Co^{2+}, Pd^{2+}, Pt^{2+}. These cations are located inside the zeolite so that, their electronic properties can experience important changes,[21] depending on the coordination environment, the Si/Al ratio, the zeolite framework, etc. Metal exchanged zeolites are prepared by ion exchange of the commercial form, normally with Na^{+} or H^{+} cations. This ion exchange is done by adding a salt of the desired cation. For example, copper Cu^{2+} cations are introduced using $Cu(NO_3)_2$ or $Cu(AcO)_2$,[22-25] Cu^{+} cations using CuCl[26,27] and Pd^{2+} and Pt^{2+} using salts which contain the cation complexed as $[Pd(NH_3)_4]^{2+}$ and $[Pt(NH_3)_4]^{2+}$ followed by thermal elimination of the ammonia ligand.[28]

Another important point to consider is that a zeolite has a high surface area, but this area is mainly internal, inside the channels or cavities, where the catalytic sites are normally located. This is an unusual characteristic for solid materials and has consequences in reaction or adsorption selectivity.[1,8,18,20] Molecules must diffuse through the channels before reacting or being adsorbed. Due to the channel size not all possible molecules can diffuse through them. Moreover, from a mixture of possible products, only those with the appropriate size or shape will be formed and diffuse out of the zeolite. Finally, only those reactions involving a transition state structure that is favoured by the environment of the active site of the zeolite will be produced. That is, those reactions for which transition state structures are stabilized will be preferred.

Due to their properties, zeolites have been used as ion exchangers, molecular sieves or catalysts.[1,5,7] Their use as ion-exchange solids comes from the capability of

zeolites to easily exchange the extra-framework cations in solution. This ion exchange capability has been applied in detergency as water softeners, that is, the zeolite captures Ca^{2+} and Mg^{2+} cations from the water by exchange with its alkali metal cations. Moreover, they can also be used in wastewater treatments to remove some undesired ions as ammonium or even as radioisotope scavengers.[1,7]

The use of zeolites as molecular sieves is based on their capability to reversibly adsorb molecules inside their pores. Molecules inside zeolite's channels experience interactions that vary depending on the Si/Al ratios.[4] For low Si/Al ratios with a large number of compensating cations the electrostatic interactions are predominant. Because of that, they preferentially adsorb polar molecules. On the other hand, interactions in zeolites with high Si/Al ratios are mainly driven by dispersion forces, so that non-polar molecules are preferably adsorbed. Furthermore, the shape and size of the channels also control the molecules that could diffuse inside the zeolite, that is, only molecules with smaller size than that of the channel and appropriate shape would be able to diffuse inside the zeolite.

Nowadays, zeolites are applied as powerful desiccants, in gas purification processes, such as the removal of CO_2, H_2S or nitrogen products in natural gas.[1,7,18] Moreover, they have been used in several separation processes of gases and liquids. As an example, it is worth mentioning that certain zeolites are able to separate gas mixtures of n- and iso-alkanes.[11] Furthermore, their ability for storage and transport of several gases such as H_2 and CH_4 has been studied.[29]

Zeolites are among the most used heterogeneous catalysts in industry, especially in petrochemistry.[1] Zeolite catalysts can be classified in two main groups: a) proton exchanged zeolites, which are widely used in acid-base catalysis and b) zeolites with transition metals cations, which are normally related with oxidation and/or reduction processes. Zeolites with both transition metal cations and acid centres are also found in the literature and thus they can present both acid and redox properties.

Acidic zeolites present catalytic activity in many organic processes.[2,4,18,20,30] Some examples are cracking, hydrocracking and skeletal reorganization in petrochemistry, olefin isomerization and oligomerization, additions, substitutions and eliminations,

mainly with olefins and finally condensation reactions. A special case of this last group of reactions is the aldol condensation produced in acidic ZSM-5.[18]

Metal exchanged zeolites have been reported to present catalytic activity mainly in oxidation or reduction reactions.[25,30-33] They have been used in hydrogenation of olefins, in some oxidation processes of olefins to produce ketones, in combustion reactions, or in the synthesis of acetonitrile from ethane, oxygen and ammonia. Moreover, the use of metal exchanged zeolites in the decomposition of nitrogen oxides (NO_x) to N_2 and O_2 has been largely studied and several decomposition mechanisms have been reported. For NO_x decomposition, CoZSM-5 and CuZSM-5 have been found to be the most active zeolite catalysts,[31] while PdZSM-5 has been reported as a good catalyst for the NH_3 oxidation to N_2.[21]

References

(1) Dyer, A. Zeolites. In *Encyclopedia of Inorganic Chemistry*; King, R. B., Ed.; John Wiley and Sons: Chichester, 1994; Vol. 8; pp 4363.

(2) Ghobarkar, H.; Schäf, O.; Guth, U. *Prog. Solid St. Chem.* **1999**, *27*, 29.

(3) Sauer, J. Zeolites: Applications of Computational Methods. In *Encyclopedia of Computational Chemistry*; von Ragué-Schleyer, P., Ed.; John Wiley and Sons: Chichester, 1998; Vol. 5; pp 3248.

(4) Corma, A. *Chem. Rev.* **1995**, *95*, 559.

(5) Smart, L.; Moore, E. Zeolites and related structures. In *Solid State Chemistry: An Introduction*; 2nd ed.; Chapman & Hall: London, 1995; pp 238.

(6) Cronstedt, A. F.; Kongl. Vetenskaps, Acad. Handl. Stockh., 1756; Vol. 17; pp 120.

(7) Olson, R. H.; Breck, D. W.; Sheppard, R. A.; Mumpton, F. A. Zeolites. In *Industrial Minerals and Rocks*; Lefond, S. J., Ed.; Port City Press: Baltimore, 1983; Vol. 2; pp 1391.

(8) Weitkamp, J. *Solid State Ionics* **2000**, *131*, 175.

(9) Cundy, C. S.; Cox, P. A. *Chem. Rev.* **2003**, *103*, 663.

(10) Baerlocher, C.; Meier, W. M.; Olson, D. H. *Atlas of Zeolite Framework Types*; Elsevier: Amsterdam, 2001.

(11) Dent, L. S.; Smith, J. V. *Nature* **1958**, *181*, 1794.

(12) Pérez-Guerrero, D.; Buxó, P.; Maza, S.; Mirabal, R.; Ongay, M.; Ruiz-Mallén, F. M. Dipòsits de Zeolites. In *Atles d'associacions minerals en làmina prima*; Melgarejo, J.-C., Ed.; Edicions Universitat de Barcelona: Barcelona, 1997; pp 333.

(13) Kokotailo, G. T.; Lawton, S. L.; Olson, D. H. *Nature* **1978**, *272*, 437.

(14) Olson, D. H.; Kokotailo, G. T.; Lawton, S. L.; Meier, W. M. *J. Phys. Chem.* **1981**, *85*, 2238.

(15) van Koningsveld, H.; Jansen, J. C.; van Bekkum, H. *Zeolites* **1990**, *10*, 235.

(16) Argauer, R. J.; Landort, G. R. US Pat 3,702,886 (Mobil Oil Corporation), November 14, 1972.

(17) Barrer, R. M. *Hydrothermal Chemistry of Zeolites*; Academic Press: London, 1982.

(18) Hölderich, W.; Hesse, M.; Näumann, F. *Angew. Chem. Int. Ed. Engl.* **1988**, *27*, 226.

(19) Löwenstein, W. *Am. Mineralogist* **1954**, *39*, 92.

(20) Sen, S. E.; Smith, S. M.; Sullivan, K. A. *Tetrahedron* **1999**, *55*, 12657.

(21) Armor, J. N. *Micropor. and Mesopor. Mater.* **1998**, *22*, 451.

(22) Schay, Z.; Knözinger, H.; Guczi, L.; Pál-Borbély, G. *Appl. Catal. B: Environmental* **1998**, *18*, 263.

(23) Dandekar, A.; Vannice, M. A. *Appl. Catal. B: Environmental* **1999**, *22*, 179.

(24) Dědeček, J.; Sobalík, Z.; Tvarůžková, Z.; Kaucký, D.; Wichterlová, B. *J. Phys. Chem.* **1995**, *99*, 16327.

(25) Shelef, M. *Chem. Rev.* **1995**, *95*, 209.

(26) Spoto, G.; Zecchina, A.; Bordiga, S.; Ricchiardi, G.; Martra, G.; Leofanti, G.; Petrini, G. *Appl. Catal. B: Environmental* **1994**, *3*, 151.

(27) Turnes-Palomino, G.; Bordiga, S.; Zecchina, A.; Marra, G. L.; Lamberti, C. *J. Phys. Chem. B* **2000**, *104*, 8641.

(28) Xin, M.; Hwang, I. C.; Woo, S. I. *J. Phys. Chem. B* **1997**, *101*, 9005.

(29) Nijkamp, M. G.; Raaymakers, J. E. M. J.; van Dillen, A. J.; de Jong, K. P. *Appl. Phys. A* **2001**, *72*, 619.

(30) Davis, M. E. *Microporous and Mesoporous Materials* **1998**, *21*, 173.

(31) Iwamoto, M.; Hamada, H. *Catal. Today* **1991**, *10*, 57.

(32) Glebov, L. S.; Zakirova, A. G.; Tret'yakov, V. F.; Burdeinaya, T. N.; Akopova, G. S. *Pretroleum Chemistry* **2002**, *42*, 143.

(33) Centi, G.; Perathoner, S. *Appl. Catal. A: General* **1995**, *132*, 179.

2. Zeolite modelling

The study of solids such as zeolites is a challenge for computational chemistry. Four different approaches are commonly used. The simplest one consists on performing quantum chemical calculations on a small fragment of the solid, called cluster. These clusters represent the active site of the zeolite, but they do not consider the rest of the solid. To correct this deficiency larger clusters should be considered. However, the computational cost rapidly increases with the size of the cluster. Thus, alternative approaches should be applied. In particular, ONIOM[1-3] approach divides the system in two layers that are treated at different computational levels. This allows the study of larger clusters and so, to get a better description of the system. In the present thesis, those large clusters computed applying ONIOM approach will be called ONIOM clusters in order to distinguish them from small clusters (free clusters) computed using a unique level of theory. Embedded-cluster approach also divides the system in two parts, but in contrast to ONIOM clusters, the second layer includes periodic conditions to represent the whole solid. Finally, fully ab-initio periodic calculations can also be done. This approach is the best one if the level of theory used is accurate enough.

The present chapter describes in detail all of them. The order of the exposition will follow the increase of complexity, that is, free clusters, ONIOM clusters, embedded clusters and periodic calculations. For each modelling, the employed levels of theory considered will be presented and we will briefly mention some examples where they have been used in the literature.

2.1. Free clusters.

A free cluster is the simplest way to model a zeolite.[4-6] The substitution of an infinite solid by a finite cluster is justified assuming that the chemical problem studied depends mainly on local properties of the solid. In zeolites with low aluminium content, most properties are determined by the local effect produced by the Si/Al substitution. Thus, the use of a small cluster to model the zeolite has been largely used with satisfactory results.[4,7-9] Moreover, their size allows the use of accurate levels of theory such as density functional theory (DFT) or MP2.[10]

Three types of errors are made when replacing a periodic solid by a finite cluster.[5,6] First, the selected cluster may not consider the essential chemistry involved in the system.

This can be tested by increasing the cluster size and looking for converged results with cluster size. Second, constraints produced by the infinite structure are not considered. The cluster is normally fully optimised and the structure of the solid is lost. This leads to an extra stabilization of the system which is not real and could lead to wrong results. Sometimes, a constrained optimisation is imposed to fix part of the solid structure. However, these constraints are normally too strong compared to the real situation and also the localisation of stationary points becomes more difficult. Third, the long-range effects are not included in cluster calculations. In some cases, these effects may be important and so, the validity of the cluster approximation should be tested using one of the next approximations, especially those that introduce periodic conditions.

The simplest free cluster that one can find in the literature is formed by one aluminium tetrahedron.[11-14] This cluster was used in the first theoretical studies of zeolites. However, nowadays its use is rare. Di[15,16], tri[7,15,17-23] and pentatetrahedral[16-18,24-26] are the most commonly employed free clusters as they are not extremely computationally demanding and in many systems they have been shown to reproduce the main trends correctly. Recently, clusters that include small rings have also been used to model the location of metal cations in zeolites.[27-31]

2.2 ONIOM clusters

The ONIOM[1-3] (our own n-layered integrated molecular orbital and molecular mechanics) approach allows to use larger clusters. This approach subdivides the whole system (real) in different layers, normally 2 or 3, each one being described at a different level of theory. The most important part, which includes the active site of the zeolite, is called the model system and it is described at a high level of theory, whereas the rest of the zeolite cluster is computed at a lower level. When two layers are used, the total energy of the system is obtained from three independent calculations:

$$E^{ONIOM} = E^{high}_{model} + E^{low}_{real} - E^{low}_{model} \qquad (2.1)$$

This method can be viewed as an extrapolation scheme. Starting from E^{high}_{model}, the extrapolation to the real system $E^{low}_{real} - E^{low}_{model}$ is assumed to give an estimation for E^{high}_{real}.

One of the critical features of combination schemes is how bonds between atoms of different layers are treated. Normally these bonds are broken and the model part is saturated with link atoms; that is, the original bond is replaced by a new terminal one which conserves the direction of the broken real bond. Normally link atoms are hydrogens.

The atoms that belong to the model layer are fixed to have the same coordinates than the equivalent atoms of the real part. Thus, when no bond exists between the two layers the first derivative of the energy with respect to the geometry is easily obtained as the sum of the separated gradients for each calculation and so, geometry optimisations are easily performed.[2]

$$\frac{\partial E^{ONIOM}}{\partial q} = \frac{\partial E^{high}_{model}}{\partial q} + \frac{\partial E^{low}_{real}}{\partial q} - \frac{\partial E^{low}_{model}}{\partial q} \qquad (2.2)$$

The situation becomes somewhat more complicated when there are covalent bonds between layers. The link atoms do not exist in the real system and thus one of the main issues is their geometrical placement. ONIOM approach connects the link atoms of the high level layer with the same bond angles and dihedral angles as the substituted atoms of the real model. This connection introduces the steric effects of the substituents in the model system calculations. The bond length of these linking bonds is determined by scaling the bond distance between the high level part and link atoms, so that reasonable bond lengths between the two layers are obtained.

It must be pointed out that this optimisation scheme leads to structures that correspond neither to a minimum of the model part nor to a minimum of the real part, but it minimizes the E^{ONIOM} (equation 2.1) energy.

One of the most critical points of the ONIOM approach is how the system is partitioned and which combination of high and low-levels of theory should be used.[2] For this reason Vreven and Morokuma suggested a test (the s-Value test)[2] which involves the computation of the global system at the high level of theory for at least one case; that is, they suggest to compute a target value. As our ONIOM clusters are too big to compute directly the E^{high}_{real} value, when possible, we have substituted this value for the full periodic calculation and/or the experimental value. In the present thesis the level of theory for the model part is DFT (B3LYP)[32,33] while for the real part we have used HF[34,35] and semiempirical methods (MNDO[36] or AM1[37]). A description of these methods can be found in the appendix.

ONIOM clusters have not been widely used in solid-state chemistry. This kind of extrapolation schemes are used preferably in transition metal complexes with large ligands.[38-40] However, their potentiality in modelling zeolites and related materials has been suggested[41-43] as they can include a more constrained structure and take into account medium range effects such as the effect of the channel. The constraints introduced with ONIOM are not as artificial as in free clusters, so that the model becomes more realistic. For this purpose it is of great importance to avoid open $(Si-O)_n$ chains and to include small $(Si-O)_n$ rings. It must be pointed out that they are still cluster calculations, so that the global modelling of the zeolite is not done and they do not include full long-range effects.

One can find in the literature very few articles which model acidic zeolites or related materials using ONIOM and most of them have been published after the beginning of the present thesis.[41,42,44-49] The majority of these studies deal with adsorption energies of probe molecules in zeolites or related materials and some of them try to identify an appropriate high and low-level combination. Roggero et al.[41] have concluded that among several semiempirical methods combined with B3LYP, MNDO leads to better geometry parameters, while AM1 leads to better adsorption energies.

2.3 Embedded Clusters. QM-Pot

Embedded clusters are clusters which are constrained by an outer part which presents periodic boundary conditions.[4,5] That is, the local part where the majority of the chemistry is included is described at an accurate level of theory, whereas long-range effects are evaluated at a lower level. Several modellings of the long-range effects can be used. In the literature one can find the use of point charges to reproduce the Madelung constant,[50,51] the introduction of a correcting electrostatic potential,[52,53] PCM[42] and, finally, the use of force fields with periodic boundary conditions.[5,54] One example of the latter case is the QM-Pot scheme developed by Sierka and Sauer.[55,56] QM-Pot scheme is probably the embedded cluster approach that have provided more satisfactory results in a larger variety of situations.[7,57-65]

The basic idea of the QM-Pot method[5] is the same presented for ONIOM. That is, the system is divided in two parts, one is computed at an accurate level of theory while the other is computed using molecular mechanics with periodic conditions. Thus, the energy of the system is computed from:

$$E^{QM-Pot} = E^{QM}_{model} + E^{Pot}_{real} - E^{Pot}_{model} \qquad (2.3)$$

and geometry optimisations are performed with the same ONIOM procedure.

It must be said that although the described modelling has been developed for silicates and zeolites, similar approximations could be done for other systems by fitting the parameters properly. Normally the quantum mechanical part used in QM-Pot calculations is DFT or MP2, while the force field for the molecular mechanics is built starting from a shell model potential.[66] The shell model potential represents the ions of the system by a pair of point charges, the positive core and the negative and massless shell. The coordinates of the core and the shell are optimised separately but they are connected by an harmonic potential. The global interaction between these ions is approximated by:

$$E^{Pot} = E^{elec} + E^{core-shell} + E^{short-range} + E^{3-body} \qquad (2.4)$$

The first term, E^{elec}, corresponds to the Coulomb energy,

$$E^{elec} = \sum_{i,j} \frac{q_i q_j}{r_{ij}} \qquad (2.5)$$

where q_i and q_j are the formal charges of the involved shells or cores, and r_{ij} is the distance between them. The second term, $E^{core-shell}$ is the harmonic potential which connects each shell to each nucleus and is represented by:

$$E^{Core-shell} = \sum_{i} K_i r_i^2 \qquad (2.6)$$

The third term is the repulsion term between shells and cations and is expressed by the Buckingham potential[67] where the attractive term has been neglected.

$$E^{short-range} = \sum_{k.l} A_{k,l} e^{-r_{k,l}/\rho_{k,l}} \qquad (2.7)$$

Finally a three-body potential is introduced to describe the tetrahedral geometry coordination of silicon and aluminium atoms. This $E^{3\text{-body}}$ presents the following expression:

$$E^{3-body} = \frac{1}{2} \sum_{i} \sum_{j,k} k_i^b (\theta_{ijk} - \theta_o)^2 \qquad (2.8)$$

and corresponds to an harmonic potential around the ideal tetrahedral angle (θ_o = 109.47º). In the sum j and k runs over the shells of oxygen atoms that are bonded to the ith silicon or aluminium core. This last term is not common in ionic systems and it is introduced to represent the covalent character of bonds in zeolites.

As it is observed, the energy expression depends on several parameters (q_i, k_i, A_{kl}, ρ_{kl}, k_i^b) which must be fitted to describe as properly as possible a large variety of situations. This fitting has been done by comparing with Hartree-Fock or DFT calculations of several molecular models (ring clusters), using a double-ζ plus polarization basis set for Si, Al and H and a valence triple zeta plus polarization for oxygen.[66,68]

The QM-Pot scheme has been applied in a large number of studies and has provided accurate enough results. Several examples are the computation of adsorption energies of probe molecules in acidic zeolites,[59-61] the determination of absolute acidities of zeolites[62,63] and the study of metal-ligand interactions in copper exchanged zeolites.[7] Recently, QM-Pot methodology has been applied to study catalytic processes inside zeolites.[55,64,65]

Compared to the previous two approaches, the QM-Pot method introduces the periodicity of the system without increasing the computational cost. However, long-range effects are introduced indirectly and at a low level of theory. Moreover, another important disadvantage is the need of fitting the parameters of the interatomic potentials for each new situation.

2.4. Periodic calculations.

A crystalline solid contains a great number (infinite) of atoms and so, at first glance, its rigorous study seems not possible. However, the existence of periodicity allows us to study the global solid.[69]

A crystalline solid consists on the repetition of atoms or groups of atoms in the three dimensions. The motifs that by translation ($\vec{T}$) in the $\vec{a}$, $\vec{b}$, $\vec{c}$ directions generate the whole crystalline solid are called unit cells and are not unique.[70,71] Within all possible unit cells, those with the smallest volume are called primitive cells.

$$\vec{T} = u\vec{a} + v\vec{b} + w\vec{c} \qquad (2.9)$$

where $\vec{T}$ is the translational vector, u, v, w are integers ranging from minus infinity to plus infinity and $\vec{a}$, $\vec{b}$ and $\vec{c}$ are three non-coplanar vectors defining the basis of the three-dimensional space.

Several ways of constructing units cells are possible, one possibility is the union of equivalent by periodicity points of the solid (lattice points) that leads to unit cells formed by parallelepipeds. On the other hand, Wigner-Seitz unit cells[69,70] are obtained by connecting each lattice point to its nearest neighbours and tracing the planes perpendicular to these segments through their midpoints.

For periodic calculations, as well as for interpretation of many physical properties of crystals, it is useful to introduce the so-called reciprocal lattice.[69,71,72] Given a direct lattice (as defined above) we can define a new lattice by the vectors $\vec{a}^*$, $\vec{b}^*$ and $\vec{c}^*$

$$\vec{a}^* = (\vec{b}\times\vec{c})/V \qquad \vec{b}^* = (\vec{c}\times\vec{a})/V \qquad \vec{c}^* = (\vec{a}\times\vec{b})/V \qquad (2.10)$$

where $\vec{a}$, $\vec{b}$ and $\vec{c}$ are the vectors of the direct lattice, and V is the volume of the unit cell of the direct lattice. The unit cell of the reciprocal lattice obtained using the Wigner-Seitz construction is called the first Brillouin zone and it is of great importance in periodic calculations.

Periodic calculations are based on the Bloch theorem,[69,72] which states that:

$$\hat{T}\psi^{\vec{\kappa}}(\vec{r}) = \psi^{\vec{\kappa}}(\vec{r}+\vec{T}) = e^{(i\vec{\kappa}\vec{T})}\psi^{\vec{\kappa}}(\vec{r}) \qquad (2.11)$$

$\psi^{\vec{\kappa}}(\vec{r})$ are the Bloch functions, which are are adapted to the symmetry of the crystal and play the same role as that of molecular orbitals in molecular calculations, $\hat{T}$ is a translational operator, $\vec{\kappa}$ is a vector of the reciprocal lattice

$$\vec{\kappa} = \kappa_1\vec{a}^* + \kappa_2\vec{b}^* + \kappa_3\vec{c}^* \qquad (2.12)$$

and $\vec{T}$ is the translational vector which results of the application of $\hat{T}$ on $\psi^{\vec{\kappa}}(\vec{r})$.

The eigenvectors of the Hamiltonian operator of a crystalline solid are always related with a $\vec{\kappa}$ vector of the reciprocal lattice. The number of $\vec{\kappa}$ vectors is infinite. However, due to the translational symmetry of the reciprocal space, it is observed that only $\vec{\kappa}$ vectors of the Brillouin zone are not redundant. Moreover, applying periodic boundary conditions (one

assumes that the finite crystalline solid is part of an infinite solid, delimited in a purely formal way), it is obtained that,

$$\kappa_i = \frac{n_i}{N_i} \qquad (2.13)$$

where N_i is the total number of cells considered and n_i is a natural number between 1 and N_i. The number of κ values (in the Brillouin zone) is no longer infinite, and it has become equal to the number of cells in the crystal.

Bloch functions are normally constructed using a linear combination of one-electron functions.[73] Normally these one-electron functions are plane-waves (PW) or Gaussian type orbitals (GTO). PW are Bloch functions associated to a $\vec{\kappa}$ within the Brillouin zone and they are independent of the nature of the atoms and their location within the cell. GTO are atomic orbitals of the constituents of the unit cell referred to its origin. Normally diffuse functions are avoided as they may cause computational problems. Advantages of using GTO instead of PW are that they lead to a better description of the electronic distribution, chemical interpretation is easier and comparison with finite models is feasible. In the present thesis we have used Bloch functions constructed from a linear combination of GTO.

The electronic Schrödinger equation should be solved for each $\vec{\kappa}$ point. This is done using a self consistent field (SCF) for each $\vec{\kappa}$ point in a similar way to those used in molecular calculations

$$H^{\vec{\kappa}}C^{\vec{\kappa}} = S^{\vec{\kappa}}C^{\vec{\kappa}}E^{\vec{\kappa}} \qquad (2.14)$$

Up to this point the main problem is the large amount of $\vec{\kappa}$ points that should be considered. However, as eigenfunctions and eigenvalues are continuous with respect to $\vec{\kappa}$ it is possible to derive the required information from the results obtained at a few suitable sampled $\vec{\kappa}$ points. Moreover, it must be pointed out that the volume of the Brillouin zone is inversely proportional to the volume of the unit cell and thus for several systems the Brillouin zone is really small. In the present thesis 8 κ points have been considered.

It can be found in the literature several studies where zeolites are modelled with periodic calculations.[8,9,17,61,74-77] They are generally very recent and they often use PW as basis sets. To our knowledge none of them deals with transition metal exchanged zeolites and only very recently they have been used to study catalytic processes in zeolites.[8]

In the present thesis we have used the approaches described in subsections 2.1, 2.2 and 2.4. The following notation has been considered to indicate the model used. Clusters will be named indicating the number of tetrahedra which compose them. For example, the $[H_3SiOAl(OH)_2OSiH_3]$ cluster formed by three tetrahedra will be referred as T3. The clusters studied using the ONIOM scheme will be named indicating the number of tetrahedra that form the inner layer and the number of tetrahedra of the whole system. Thus, T3:T69 indicates that the inner part is formed by a T3 cluster, while the real system is formed by 69 tetrahedra. In these two cases, the zeolite will be schematically represented by Z. Finally, in periodic calculations the zeolite will be named using the IUPAC nomenclature.

References

(1) Svensson, M.; Humbel, S.; Froese, R. D. J.; Matsubara, T.; Sieber, S.; Morokuma, K. *J. Phys. Chem.* **1996**, *100*, 19357.

(2) Vreven, T.; Morokuma, K. *J. Comput. Chem.* **2000**, *21*, 1419.

(3) Maseras, F.; Morokuma, K. *J. Comput. Chem.* **1995**, *16*, 1170.

(4) Sauer, J.; Ugliengo, P.; Garrone, E.; Saunders, V. R. *Chem. Rev.* **1994**, *94*, 2095.

(5) Sauer, J.; Sierka, M. *J. Comput. Chem.* **2000**, *21*, 1470.

(6) Sauer, J. Zeolites: Applications of Computational Methods. In *Encyclopedia of Computational Chemistry*; von Ragué-Schleyer, P., Ed.; John Wiley and Sons: Chichester, 1998; Vol. 5; pp 3248.

(7) Rodríguez-Santiago, L.; Sierka, M.; Branchadell, V.; Sodupe, M.; Sauer, J. *J. Am. Chem. Soc.* **1998**, *120*, 1545.

(8) Vos, A. M.; Rozanska, X.; Schoonheydt, R. A.; van Santen, R. A.; Hutschka, F.; Hafner, J. *J. Am. Chem. Soc.* **2001**, *123*, 2799.

(9) Boronat, M.; Zicovich-Wilson, C. M.; Corma, A.; Viruela, P. *Phys. Chem. Chem. Phys.* **1999**, *1*, 537.

(10) Møller, C.; Plesset, M. S. *Phys. Rev.* **1934**, *46*, 618.

(11) Teunissen, E. H.; van Santen, R. A.; Jansen, A. P. J.; van Duijneveldt, F. B. *J. Phys. Chem.* **1993**, *97*, 203.

(12) Schneider, W. F.; Hass, K. C.; Ramprasad, R.; Adams, J. B. *J. Phys. Chem. B* **1998**, *102*, 3692.

(13) Schneider, W. F.; Hass, K. C.; Ramprasad, R.; Adams, J. B. *J. Phys. Chem. B* **1997**, *101*, 4353.

(14) Sengupta, D.; Adams, J. B.; Schneider, W. F.; Hass, K. C. *Catal. Lett.* **2001**, *74*, 193.

(15) Kassab, E.; Fouquet, J.; Allavena, M.; Evleth, E. M. *J. Phys. Chem.* **1993**, *97*, 9034.

(16) Blint, R. J. *J. Phys. Chem.* **1996**, *100*, 19518.

(17) Boronat, M.; Zicovich-Wilson, C. M.; Viruela, P.; Corma, A. *Chem. Eur. J.* **2001**, *7*, 1295.

(18) Boronat, M.; Zicovich-Wilson, C. M.; Viruela, P.; Corma, A. *J. Phys. Chem. B* **2001**, *105*, 11169.

(19) Boronat, M.; Viruela, P.; Corma, A. *J. Phys. Chem. A* **1998**, *102*, 9863.

(20) Rigby, A. M.; Frash, M. V. *J. Mol. Catal.* **1997**, *126*, 61.

(21) Blaszkowski, S. R.; Nascimento, M. A. C.; van Santen, R. A. *J. Phys. Chem.* **1996**, *100*, 3463.

(22) Sierraalta, A.; Añez, R.; Brussin, M.-R. *J. Catal.* **2002**, *205*, 107.

(23) Tajima, N.; Hashimoto, M.; Toyama, F.; El-Nahas, A. M.; Hirao, K. *Phys. Chem. Chem. Phys.* **1999**, *1*, 3823.

(24) Khaliullin, R. Z.; Bell, A. T.; Kazansky, V. B. *J. Phys. Chem. A* **2001**, *105*, 10454.

(25) Rice, M. J.; Chakraborty, A. K.; Bell, A. T. *J. Phys. Chem. A* **1998**, *102*, 7498.

(26) Trout, B. L.; Chakraborty, A. K.; Bell, A. T. *J. Phys. Chem.* **1996**, *100*, 17582.

(27) Delabie, A.; Pierloot, K.; Groothaert, M. H.; Schoonheydt, R. A.; Vanquickenborne, L. G. *Eur. J. Inorg. Chem.* **2002**, 515.

(28) Delabie, A.; Pierloot, K.; Groothaert, M. H.; Weckhuysen, B. M.; Schoonheydt, R. A. *Micropor. and Mesopor. Mater.* **2000**, *37*, 209.

(29) Delabie, A.; Pierloot, K.; Groothaert, M. H.; Weckhuysen, B. M.; Schoonheydt, R. A. *Phys. Chem. Chem. Phys.* **2002**, *4*, 134.

(30) Pierloot, K.; Delabie, A.; Ribbing, C.; Verberckmoes, A. A.; Schoonheydt, R. A. *J. Phys. Chem. B* **1998**, *102*, 10789.

(31) Berthomieu, D.; Krishnamurty, S.; Coq, B.; Delahay, G.; Goursot, A. *J. Phys. Chem. B* **2001**, *105*, 1149.

(32) Becke, A. D. *J. Chem. Phys.* **1993**, *98*, 5648.

(33) Lee, C.; Yang, W.; Parr, R. G. *Phys. Rev. B* **1988**, *37*, 785.

(34) Hartree, D. R. *Proc. Cambridge Phil. Soc.* **1928**, *24*, 89.

(35) Fock, V. *Z. Physik* **1930**, *61*, 126.

(36) Dewar, M. J. S.; Thiel, W. *J. Am. Chem. Soc.* **1977**, *99*, 4899.

(37) Dewar, M. J. S.; Zoebisch, E. G.; Healy, E. F.; Stewart, J. J. P. *J. Am. Chem. Soc.* **1985**, *107*, 3902.

(38) Maseras, F. *Chem. Commun.* **2000**, 1821.

(39) Maseras, F.; Lledós, A.; Clot, E.; Eisenstein, O. *Chem. Rev.* **2000**, *100*, 601.

(40) Maseras, F.; Lledós, A. Computational Modeling for Homogeneous Catalysis. In *Computational Modeling of Homogeneous Catalysis*; Maseras, F., Lledós, A., Eds.; Kluwer Academic Publishers: Dordrecht, 2002; Vol. 25; pp 384.

(41) Roggero, I.; Civalleri, B.; Ugliengo, P. *Chem. Phys. Lett.* **2001**, *341*, 625.

(42) Erbetta, D.; Ricci, D.; Pacchioni, G. *J. Chem. Phys.* **2000**, *113*, 10744.

(43) Lopez, N.; Pacchioni, G.; Maseras, F.; Illas, F. *Chem. Phys. Lett.* **1998**, *294*, 611.

(44) Ricci, D.; Pacchioni, G.; Szymanski, M. A.; Shluger, A. L.; Stoneham, A. M. *Phys. Rev. B* **2001**, *64*, 224104.

(45) Sillar, K.; Burk, P. *Theochem* **2002**, *589-590*, 281.

(46) Bonino, F.; Damin, A.; Bordiga, S.; Lamberti, C.; Zecchina, A. *Langmuir* **2003**, *19*, 2155.

(47) Bordiga, S.; Damin, A.; Bonino, F.; Zecchina, A.; Spanò, G.; Rivetti, F.; Bolis, V.; Prestipino, C.; Lamberti, C. *J. Phys. Chem. B* **2002**, *106*, 9892.

(48) Damin, A.; Bordiga, S.; Zecchina, A.; Lamberti, C. *J. Chem. Phys.* **2002**, *117*, 226.

(49) Raksakoon, C.; Limtrakul, J. *J. Mol. Struct.: Theochem* **2003**, *631*, 147.

(50) Kyrlidis, A.; Cook, S. J.; Chakraborty, A. K.; Bell, A. T.; Theodorou, D. N. *J. Phys. Chem.* **1995**, *99*, 1505.

(51) Vollmer, J. M.; Stefanovich, E. V.; Truong, T. N. *J. Phys. Chem. B* **1999**, *103*, 9415.

(52) Teunissen, E. H.; Jansen, A. P. J.; van Santen, R. A. *J. Phys. Chem.* **1995**, *99*, 1873.

(53) Teunissen, E. H.; Jansen, A. P. J.; van Santen, R. A.; Orlando, R.; Dovesi, R. *J. Chem. Phys.* **1994**, *101*, 5865.

(54) de Vries, A. H.; Sherwood, P.; Collins, S. J.; Rigby, A. M.; Rigutto, M.; Kramer, G. J. *J. Phys. Chem. B* **1999**, *103*, 6133.

(55) Sierka, M.; Sauer, J. *J. Chem. Phys.* **2000**, *112*, 6983.

(56) Eichler, U.; Kölmel, C. M.; Sauer, J. *J. Comput. Chem.* **1996**, *18*, 463.

(57) Nachtigall, P.; Nachtigallová, D.; Sauer, J. *J. Phys. Chem. B* **2000**, *104*, 1738.

(58) Nachtigallová, D.; Nachtigall, P.; Sierka, M.; Sauer, J. *Phys. Chem. Chem. Phys.* **1999**, *1*, 2019.

(59) Brändle, M.; Sauer, J. *J. Mol. Catal. A: Chemical* **1997**, *119*, 19.

(60) Brändle, M.; Sauer, J. *J. Am. Chem. Soc.* **1998**, *120*, 1556.

(61) Brändle, M.; Sauer, J.; Dovesi, R.; Harrison, N. M. *J. Chem. Phys.* **1998**, *109*, 10379.

(62) Eichler, U.; Brändle, M.; Sauer, J. *J. Phys. Chem. B* **1997**, *101*, 10035.

(63) Sierka, M.; Eichler, U.; Datka, J.; Sauer, J. *J. Phys. Chem. B* **1998**, *102*, 6397.

(64) Clark, L. A.; Sierka, M.; Sauer, J. *J. Am. Chem. Soc.* **2003**, *125*, 2136.

(65) Sierka, M.; Sauer, J. *J. Phys. Chem. B* **2001**, *105*, 1603.

(66) Schröder, K.-P.; Sauer, J. *J. Phys. Chem.* **1996**, *100*, 11043.

(67) Jensen, F. *Introduction to Computational Chemistry*; John Wiley and Sons: Chichester, 2002.

(68) Sierka, M.; Sauer, J. *Faraday Discuss.* **1997**, *106*, 41.

(69) Illas, F.; Ricart, J. M. Química Cuántica en Materia Condensada: Aplicación al estudio de superfícies, quimisorción, catálisi heterogénea y propiedades de sólidos. In *Química Teórica y computacional*; Andrés, J., Bertran, J., Eds.; Publicacions de la Universitat Jaume I: Castelló de la Plana, 2000; pp 217.

(70) Viterbo, D. Crystal Lattices and Crystal Symmetry. In *Quantum-Mechanical Ab-initio Calculation of the Properties of Crystalline Materials*; Pisani, C., Ed.; Springer-Verlag, 1996; pp 1.

(71) Solans, X. *Introducció a la cristal·lografia*; Edicions de la Universitat de Barcelona: Barcelona, 1999.

(72) Dovesi, R. The Language of Band Theory. In *Quantum-Mechanical Ab-initio Calculation of the Properties of Crystalline Materials*; Pisani, C., Ed.; Springer-Verlag, 1996; pp 31.

(73) Pisani, C. Ab-initio Approaches to the Quantum-Mechanical Treatment of Periodic Systems. In *Quantum-Mechanical Ab-initio Calculation of the Properties of Crystalline Materials*; Pisani, C., Ed.; Springer-Verlag, 1996; pp 47.

(74) Rozanska, X.; van Santen, R. A.; Demuth, T.; Hutschka, F.; Hafner, J. *J. Phys. Chem. B* **2003**, *107*, 1309.

(75) Pascale, F.; Ugliengo, P.; Civalleri, B.; Orlando, R.; D'Arco, P.; Dovesi, R. *J. Chem. Phys.* **2002**, *117*, 5337.

(76) Ugliengo, P.; Civalleri, B.; Zicovich-Wilson, C. M.; Dovesi, R. *Chem. Phys. Lett.* **2000**, *318*, 247.

(77) Shah, R.; Payne, M. C.; Lee, M.-H.; Gale, J. D. *Science* **1996**, *271*, 1395.

3. NO decomposition by CuZSM-5

3.1 Introduction

3.1.1 Environmental problem

Nowadays, the principal atmospheric pollutants are CO_x, SO_x, H_2S, hydrocarbons and NO_x.[1] Undesired nitrogen oxides (N_2O, NO, NO_2, N_2O_4,...) are mainly produced in high-temperature combustions of fossil fuels (petroleum, gas and coal), which take place in a great variety of industrial processes and inside vehicle engines. Thus, their effects are more important in cities and industrial areas.[2-4] About 90% of the NO_x produced in these combustions is NO.[5] However, in the atmosphere NO partially reacts with oxygen forming NO_2.

These oxides, NO and NO_2, are paramagnetic and highly reactive. They are toxic at high concentrations[6] and in the presence of water in the atmosphere they lead to HNO_2 and HNO_3, a very acid and oxidant mixture which is one of the components of the well-known acid rain.[4,5] Furthermore, some photochemical reactions of these gases in the atmosphere have been reported. In particular, it is known that, in the presence of water and hydrocarbons, such gases essentially produce an important increase of the ozone concentration in the low atmosphere layers, which is very nocive.[2,3]

NO_x are thermodynamically unstable with respect to decomposition to N_2 and O_2.[4] However they are kinetically stable and the decomposition can only take place in the presence of an appropriate catalyst. The direct decomposition reaction of NO is represented in equation 3.1

$$2NO \xrightarrow{Cat} N_2 + O_2 \qquad (3.1)$$

In addition to the direct NO decomposition, it has been also been developed the selective catalytic reduction (SCR).[6] This process consists on adding a reducing agent in the reactor, normally hydrogen, carbon monoxide, ammonia or hydrocarbons, and oxygen that induces the NO reduction to N_2 and O_2. The advantages of the direct decomposition are the absence of other products besides oxygen and nitrogen and the fact that there is no need to add other agents in the reduction process. Consequently, although nowadays most of the applied catalysts are based on the SCR process, the study of a good catalyst for the direct NO decomposition is of interest.

The studied catalysts are divided in three main groups:[4] a) noble metals such as Rh and Pt, b) metal oxides, mainly of transition metals, and perovskites (Co_3O_4, La_2O_3, Mn_2O_3 or CuO) and c) metal exchanged zeolites. Within metal exchanged zeolites CuZSM-5 has been reported as the most active catalyst for the direct NO decomposition.[4,6-8]

3.1.2. Experimental studies of the direct NO decomposition by CuZSM-5

From an experimental point of view great efforts have been done to understand the catalytic activity of Copper exchanged ZSM-5 as well as to establish the best conditions for the catalytic activity. Most of these studies are based on spectroscopic techniques such as IR, UV-VIS, EPR or XSAF.[6,7]

IR spectroscopy is used to identify the nitrogen oxides formed during the process as well as to analyse how they interact with copper. This is done by the assignment of the IR bands of the ligand to different species. Photolumiscence is used to identify and determine the cationic sites. Moreover, EPR experiments are used to determine the redox properties of copper cations coordinated to the zeolite framework, since it is thought that they may be essential during the global process. This can be done because Cu^{2+} and a great variety of the formed intermediates are paramagnetic and consequently present a characteristic EPR signal. The shape of the signal is then related with the geometry around these copper ions. X-Ray techniques are also used to determine the nature of the active site.

The first studies tried to establish the most appropriate conditions to perform the NO decomposition using CuZSM-5 as a catalyst.[4-6,9] Several factors have been considered: the Si/Al ratio, the copper exchange ratio and the effect of temperature. It has been observed that poor aluminium zeolites present higher activity for the NO decomposition. Some researchers have concluded that 50 is an idoneous Si/Al ratio. However, an acceptable conversion rate is obtained when the ratio is higher than 30.[9] Moreover, the amount of Cu^{2+} cations which are exchanged is higher than that needed to neutralize the negative charge generated by aluminium substitution. The ideal exchange percentage is around 150%.[4] Thus, the reduction of part of these cations has been suggested.

The effect of temperature has been widely studied.[4-6,9] At low and room temperatures neither O_2 nor N_2 are formed and the observed species are N_2O and NO_2. When one increases the temperature the amount of molecular nitrogen and oxygen increases until a maximum located at 773 K while the concentration of N_2O and NO_2 decreases. After the maximum at 773 K the conversion of NO to O_2 and N_2 decreases slowly. This is schematically represented in Figure 3.1.

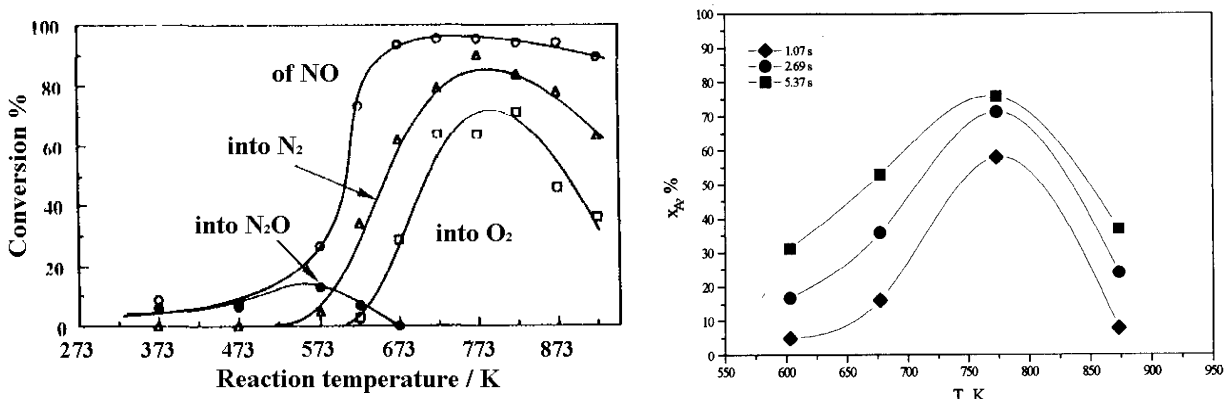

Figure 3.1 NO decomposition as a function of temperature and time[4,6]

Alternatively, several researchers have worked on the catalytic activity of CuZSM-5 at a molecular level. That is, they have focused on studying the possible active sites, as well as on the intermediates involved in the decomposition process. In spite of all the efforts that have been done, the nature of the active site in CuZSM-5 is poorly understood. Several possible active species have been detected but no conclusive experiments can be found in the literature.[9-20] Both Cu^+ and Cu^{2+} have been detected in CuZSM-5.[6] Cu^{2+} cations have been suggested to be located in small five or six-membered rings where they can be coordinated to at least three different oxygens. In addition, Cu^+ cations can be found at different sites.[12,21] On one hand, highly coordinated Cu^+ cations are located in similar rings to those where Cu^{2+} cations are found and, on the other hand, less saturated Cu^+ cations are located in the wider 10 membered rings. The later Cu^+ cations are thought to be coordinated to only two oxygens and so, they are expected to be more reactive.[12,21] Also, small $[Cu\text{-}O\text{-}Cu]^{2+}$ clusters have been detected and postulated to be the active sites.[9-11] Finally, EPR experiments suggest that the

intermediate species are in a square planar or square based pyramid species environment.[15,20]

Many IR experiments have been done to determine the nature of the intermediate species.[9,16,18,19,22-29] The detected species differ according to the experimental conditions. However, nearly all published articles have reported the existence of $(NO)_2CuZ$ and $(NO_2)CuZ$ species, especially at low temperatures. Moreover, (O)Cu, (NO)(O)CuZ, $(NO)(NO_2)CuZ$ or $(N_2O_3)CuZ$, $(NO_3)CuZ$ and $(N_2O)CuZ$ have also been identified by several authors.

All these available data led to postulate different mechanisms for the direct NO decomposition.[16,19,22,25-27] Among all proposed mechanisms, three of them have been more accepted and more widely discussed. First, the direct decomposition from dinitrosil species (mechanism A) was considered,[27]

Mechanism A

$$ZCu + 2NO \longrightarrow ZC(NO)_2 \qquad (A.1)$$

$$ZCu(NO)_2 \longrightarrow ZCu + N_2 + O_2 \qquad (A.2)$$

The other two proposed mechanisms start with the formation of (O)CuZ, which is postulated to be formed from the addition of two NO to CuZ, which dissociates into (O)CuZ and N_2O.[19,22,26]

$$CuZ + 2NO \longrightarrow (NO)_2CuZ \qquad (3.2)$$

$$(NO)_2CuZ \longrightarrow (O)CuZ + N_2O \qquad (3.3)$$

Afterwards, Aylor et al., and other groups suggested the following mechanism, which hereafter will be referred as mechanism B:[16,22]

Mechanism B

$$(O)CuZ + ON_2 \longrightarrow (O_2)CuZ + N_2 \qquad (B.1)$$

$$(O_2)CuZ \longrightarrow CuZ + O_2 \qquad (B.2)$$

This mechanism indicates that the generated N_2O interacts with (O)CuZ through the oxygen to form (O_2)CuZ and N_2. Desorption of molecular oxygen would lead to the desired products.

The IR observation of (NO_2)CuZ and other similar species led Spoto et al. and other groups to suggest a new mechanism that will be called hereafter mechanism C.[12,19,23]

Mechanism C

$$(O)CuZ + NO \longrightarrow (NO_2)CuZ \qquad (C.1)$$

$$(NO_2)CuZ + NO \longrightarrow (NO_2)(NO)CuZ/(N_2O_3)CuZ \qquad (C.2)$$

$$(NO_2)(NO)CuZ/(N_2O_3)CuZ \longrightarrow (O)CuZ + N_2 + O_2 \qquad (C.3)$$

This mechanism starts with the addition of two NO molecules to (O)CuZ to form (NO_2)CuZ first and then $(NO_2)(NO)$CuZ or (N_2O_3)CuZ. These latter species have been suggested to be the relevant intermediates in the formation of N_2 and O_2. This last mechanism is based on the observed species and on the fact that the reaction of (O)CuZ with NO seems more probable since the reaction takes place in a NO atmosphere. However, the last step, which involves a great electronic and structural rearrangement, is not well understood.

The formation of N_2O during the process has also been described.[22] This N_2O can also be decomposed to N_2[30] both through the process described in equation (B.1) or through the spin forbidden dissociation of (N_2O)CuZ represented in equation 3.4.

$$ZCu(N_2O) \longrightarrow ZCuO + N_2 \qquad (3.4)$$

3.1.3. Theoretical studies of the direct NO decomposition by CuZSM-5

Most of the theoretical studies of Cu exchanged zeolites are based on the cluster approach to model the zeolite.[31-48] To our knowledge only Treesukol[49] et al. and Sauer[50-52] et al. have included long-range effects on Cu exchanged zeolites using hybrid QM/MM schemes. Many of these studies focus on the location of Copper cations inside the zeolite and on the determination of their coordination environment.[36,37,50,51] Results agree with available experimental data, indicating that Cu^+ cations present two types of coordination environments: those where Cu^+ are coordinated to two oxygen atoms and those where Cu^+ are more saturated.[51] Cu^{2+} cations have also been studied and the results show that they normally present higher coordination numbers.[43,45-48] Simultaneously, the adsorption of small probe molecules such as NO, CO, N_2 or O_2 over Cu^+ cations in zeolite models has also been considered.[31,33,38,42,52]

Several articles related with the NO decomposition mechanism have appeared in the literature.[32,34,35,39-41] Trout et al.[35] reported the thermochemistry of a great number of possible involved reactions and they determined the most stable species. They concluded that the $(NO_2)CuZ$ species is very stable while $(NO_2)(NO)CuZ$ lies 88.2 kcal/mol above $(NO_2)CuZ$ + NO asymptote.

The first theoretical study that considers one of the postulated mechanisms referred to the direct decomposition of dinitrosil $(NO)_2CuZ$ species. Schneider et al.[39] concluded that the conversion barrier inside the zeolite is high and very similar to that computed for the gas phase reaction. Thus, the direct dinitrosil decomposition should not be considered the catalytic mechanism.

Afterwards, the same authors[40,41] as well as Tajima et al.[34] studied mechanism B. Results differ slightly since the zeolite modelling and the level of theory were not equal but they both found the same $[(NNOO)CuZ]^‡$ transition state structure for the first step. Schneider et al. used the small $Cu[Al(OH)_4]$ cluster as a model for the zeolite active site and found that the highest energy barrier is 36 kcal/mol. Thus, the postulated mechanism might explain the catalytic activity.[40,41] Although this mechanism does not occur through the most stable structures, all the considered species were found to be more stable than the CuZ + 2NO asymptote. They suggested that the more stable structures, such as $(NO_2)CuZ$, would be too stable to be involved in the decomposition process. More

recently, Tajima and co-workers[34] have improved the calculations performed by Schneider et al. using a bigger cluster (T3). They have also concluded that mechanism B might explain the catalytic effect of CuZSM-5, the highest obtained barrier (38.2 kcal/mol) being very similar to that computed by Schneider et al. (36 kcal/mol). Larger differences between both studies are observed in the relative energies of some intermediates, especially for (O)CuZ + N_2O species.

Finally, Sengupta et al.[32] have studied the formation of N_2 from (N_2O)CuZ through a spin forbidden dissociation. They estimate that the singlet-triplet crossing point lies around 23 kcal/mol above (N_2O)CuZ.

Until this thesis, the postulated mechanism C had never been studied from a theoretical point of view. Only the study of some of the involved species could be found in the literature. In particular, our group studied the (NO_2)CuZ species before the beginning of the present thesis.[52] The goals of the (NO_2)CuZ study was to determine if a T3 cluster was accurate enough to study Cu^+ exchanged zeolites and also to determine the electronic structure and stability of (NO_2)CuZ. To test the accuracy of the cluster, embedded QM/MM cluster calculations using the QM/Pot hybrid scheme[53,54] of Sierka and Sauer were also performed. The obtained results showed that both cluster and embedded cluster approaches lead to very similar results, interaction energy differences being less than 1 kcal/mol and geometry parameters being almost identical. Moreover, it was found that (NO_2)CuZ is a very stable species and thus its potential involvement in the NO_x decomposition to N_2 and O_2 should be studied.

3.2 Goal

The aim of the present chapter is to analyse the viability of mechanism C, taking as the catalytic species (O)CuZ where Cu^+ cation is coordinated to two oxygen atoms of the zeolite framework. For this purpose and due to the fact that the (NO_2)CuZ specie was previously studied, we first analyse the electronic structure and stability of (NO)(NO_2)CuZ and (N_2O_3)CuZ species, considering several possible conformers and both singlet and triplet states.

Afterwards, the decomposition of these species, which have been postulated as rellevant intermediates, is studied. Several pathways such as the direct decomposition of $(NO_2)(NO)CuZ$ or $(N_2O_3)CuZ$ to products or multi-step decomposition processes are considered. The analysis of a multi-step processes has led us to study several other possible intermediates.

3.3 Computational details

The zeolite is modelled by the same tritetrahedral $[H_3SiOAl(OH)_2OSiH_3]$ cluster (T3) used in a previous study of the coordination of NO_2 to Cu^+ in zeolites.[52]

Molecular geometries and harmonic vibrational frequencies are computed using B3LYP.[55,56] The employed basis sets are equal to those used in the $(NO_2)CuZ$ study and corresponds to those optimised by Ahlrichs and co-workers.[57] For Cu, O and N we have used triple-ζ plus polarization basis sets, while for Si, Al and H we have used double-ζ plus polarization basis sets. Thermodynamic corrections have been obtained at 298.15 K and 1 atm assuming an ideal gas, unscaled harmonic vibrational frequencies, and the rigid rotor approximation by standard statistical methods. To analyse the nature of the bonding, we have used natural population analysis of Weinhold et al.[58] All calculations have been performed with the GAUSSIAN94[59] and GAUSSIAN98[60] packages, except the CASSCF(20,14)[61] calculations of $[Cu\text{-}N_2O]^+$ spin forbidden decomposition, which have been performed with the MOLPRO program[62],

3.4 Results and discussion

Results will be presented in the following way. First, we will present the structure $(NO_2)(NO)CuZ$ and $(N_2O_3)CuZ$ as they have been suggested to be important intermediates in mechanism C. Afterwards, the study of several other species that might be involved in the mechanism will be presented. Finally the decomposition process through these intermediates will be discussed.

3.4.1. The $(NO_2)(NO)CuZ$ and $(N_2O_3)CuZ$ species.

The formation of $(NO_2)(NO)CuZ$ can be viewed as the interaction of NO with $(NO_2)CuZ$. As observed in reference 52 the preferred coordination of NO_2 to CuZ is the η^2-O,O one. This leads to a square-planar coordination around copper (Figure 3.2). The electronic ground state for this system was found to be $^2A''$, the open-shell orbital lying on the CuO_4 coordination plane. A similar bonding was found for the $Cu(NO_2)_2$ system for which the most stable structure has D_{2h} symmetry with a coplanar η^2-O,O coordination for the two NO_2 ligands.[63]

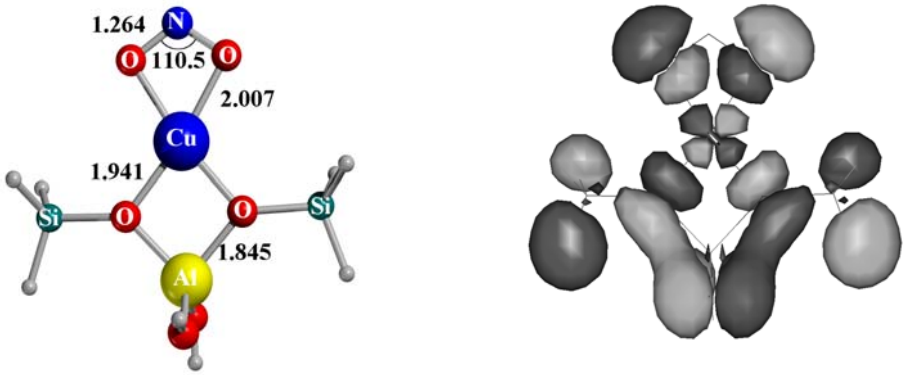

Figure 3.2 NO_2CuZ optimised structure and open shell orbital. Distance in Å, angles in degrees[52]

Since both $(NO_2)CuZ$ and NO have a doublet ground state, the resulting $(NO_2)(NO)CuZ$ system can either be in a singlet or in a triplet state, and so, we have considered both electronic states. Figure 3.3 shows the $(NO_2)(NO)CuZ$ optimised triplet structures while Figure 3.4 presents the singlet ones. The addition of the NO molecule to $(NO_2)CuZ$ can lead to a five-coordinated system, if the η^2-O,O coordination of NO_2 is retained in the final complex, or to four-coordinated systems, if NO_2 changes its coordination mode from η^2-O,O to η^1-O. For these structures all possible relative orientations of NO_2 and NO have been considered as starting points in the optimisation processes. Finally, different coordination modes of N_2O_3 to CuZ have also been analysed both in the singlet and triplet states.

Among all the structures explored, only five triplet structures (**3a-3e**) and six singlet structures (**1a-1f**) have been found to be minima on the respective potential energy surfaces. Both for the singlet and triplet spin multiplicities, **a** to **d** correspond to

$(NO_2)(NO)CuZ$ structures while **e** and **f** species are those formed by the interaction of N_2O_3 with CuZ. Within each spin multiplicity the order follows the increasing order of energy. Relative energies with respect to the most stable structure (**3a**) are given in Table 3.1. This structure is 57.7 kcal/mol more stable than (O)CuZ (^{3}A") + 2NO ($^2\Pi$) ground-state asymptote. Net atomic charges and spin densities obtained from natural population analysis are shown in Table 3.2.

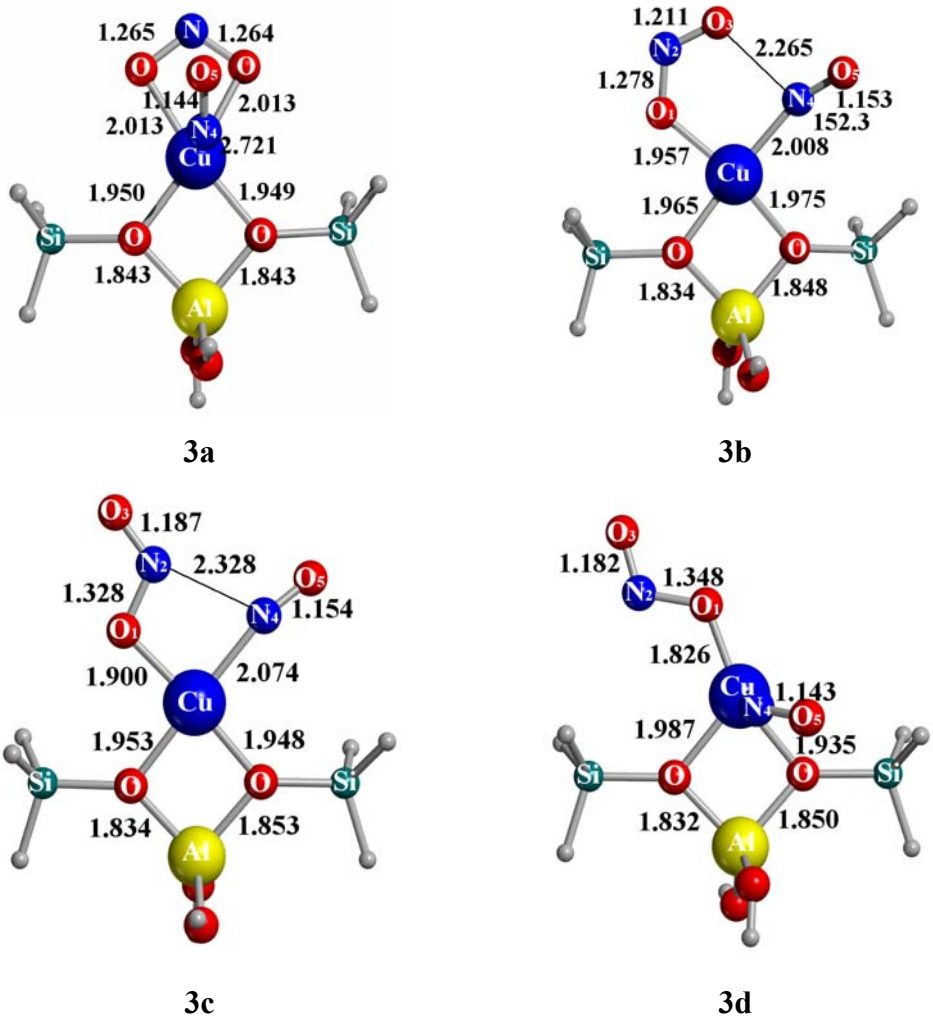

Figure 3.3 Optimised $(NO_2)(NO)CuZ$ triplet structures. Distances in Å, angles in degrees

Let us first consider the triplet structures. The lowest **3a** structure is a square pyramid with NO at the apical position. The bonding in this system can be viewed as the interaction of the ground-state structure of $(NO_2)CuZ$ with NO. That is, as in $(NO_2)CuZ$,

NO_2 acts as a bidentate ligand, interacting through the two oxygen atoms, the NO_2-CuZ bonding having a significant NO_2^--$Cu^{2+}Z^-$ ionic contribution. NO binds to (NO_2)CuZ through the nitrogen atom. The bonding energy between (NO_2)CuZ and NO is only 2.4 kcal/mol, so that the interaction is very weak. This is not surprising considering the large Cu-NO distance. The geometry parameters, the net atomic charges and spin densities of the (NO_2)CuZ fragment in the complex are very similar to those obtained for (NO_2)CuZ. Moreover, the NO geometry in the complex is very close to that of isolated NO.[64] The open shell orbitals correspond to the π^* orbital of NO which is perpendicular to the Cu coordination plane and to the open shell of (NO_2)CuZ. Thus, the 2.4 kcal/mol bonding energy mainly arises from electrostatic interaction between the NO ligand and the positive charge of Cu.

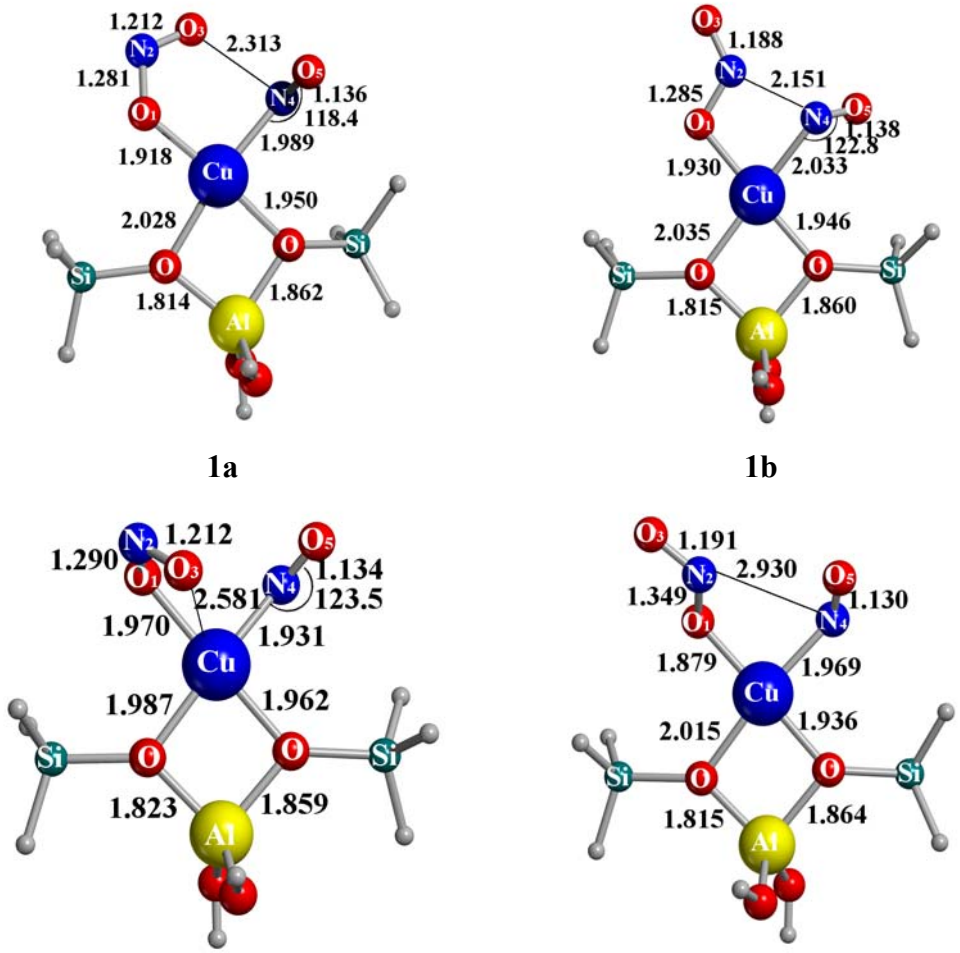

Figure 3.4 Optimised $(NO_2)(NO)$CuZ singlet structures. Distance in Å , angles in degrees

The **3b** and **3c** structures present a square-planar coordination. In these structures, NO_2 loses the bidentate coordination to allow the NO in-plane coordination. As for **3a**, the NO and (NO_2)CuZ spin populations are not far from the ones corresponding to isolated fragments. Population analysis also shows that NO has a slightly negative charge (see Table 3.2), which produces a small increase of the N-O bond length with respect to that in free NO. Thus, in these cases, the nature of the bonding is also mainly electrostatic. However, it can be observed in Figure 3.2 that the Cu-N_4 distance in **3b** and **3c** is much smaller than in **3a**. This is due to the fact that metal-NO repulsion is larger in **3a** than in **3b** or **3c**, since the metal d-orbitals pointing to NO in **3a** are doubly occupied, whereas in **3b** and **3c** the metal 3d-orbital directed towards NO is singly occupied. Although the electrostatic interaction between (NO_2)CuZ and NO in **3b** and **3c** is larger than in **3a**, the latter is the most stable structure we have obtained. This is partly due to the fact that **3a** maintains the great stabilisation of the (NO_2)CuZ bidentate structure, the larger NO-(NO_2)CuZ interaction in **3b** and **3c** not being strong enough to compensate the stability loss due to the NO_2 coordination change. The difference between **3b** and **3c** arises basically from the ligand-ligand interaction.

Table 3.1 . Relative energies to **3a** (in kcal/mol) of $(NO_2)(NO)$CuZ and (N_2O_3)CuZ species. **3a** structure lies 57.7 kcal/mol under the (O)CuZ (^{3}A") + 2NO ($^2\Pi$) asymptote.

Structure	ΔE	Structure	ΔE
3a	0.0	**1a**	0.7
3b	5.6	**1b**	2.8
3c	10.3	**1c**	3.4
3d	12.0	**1d**	8.6
3e	6.9	**1e**	11.0
		1f	12.1

Finally, **3d** has a structure similar to that of **3a**, but they differ from each other in the NO_2 coordination mode. The energy difference between **3a** and **3d** (12.0 kcal/mol) is

almost the same as the one determined between the η^2-O,O bidentate and η^1-O monodentate structures of $(NO_2)CuZ$ (12.4 kcal/mol).[52]

Table 3.2 Natural Population Analysis for $(NO_2)(NO)CuZ$ and $(N_2O_3)CuZ$ species

	Charge					Spin				
Structure	Z	Cu	NO_2	NO	N_2O_3	Z	Cu	NO2	NO	N_2O_3
3a	–0.74	1.34	–0.62	0.02		0.17	0.66	0.19	0.97	
3b	–0.74	1.32	–0.47	–0.10		0.17	0.57	0.26	1.00	
3c	–0.71	1.40	–0.56	–0.13		0.15	0.64	0.16	1.05	
3d	–0.78	1.32	–0.56	0.02		0.14	0.58	0.31	0.97	
3e	–0.72	1.40			–0.68	0.19	0.64			1.17
1a	–0.76	1.17	–0.50	0.09						
1b	–0.79	1.17	–0.41	0.04						
1c	–0.75	1.17	–0.55	0.12						
1d	–0.74	1.21	–0.63	0.16						
1e	–0.88	0.98			–0.10					
1f	–0.89	0.98			–0.09					

Let us now consider the $(NO_2)(NO)CuZ$ singlet structures (Figure 3.4). The most stable structure **1a** shows a square-planar coordination. NO_2 acts as a monodentate ligand interacting through one of the oxygen atoms, and NO binds through the nitrogen atom. As for the triplet structures, the NO_2-CuZ bonding shows a significant ionic contribution. However, $(NO_2)CuZ$ and NO form a covalent bond. In the $^2\Pi$ ground state of free NO the unpaired electron lies on the antibonding π^* orbitals, which are polarized towards the nitrogen atom. To allow the formation of a covalent bond between the unpaired electron of NO and the open shell orbital of $(NO_2)CuZ$, NO interacts forming a Cu-NO angle of 118.4º. This angle is similar in all singlet structures. Figure 3.5 shows the bonding molecular orbital that arises from this interaction. As a result, there is some electron donation from NO to $(NO_2)CuZ$ (see Table 3.2), which produces a decrease of the NO bond length compared to that of free NO. A similar decrease is found for Cu^+- NO. The

other NO π^* orbital remains unoccupied and it is directed to the O_3 atom leading to a stabilizing interaction between ligands.

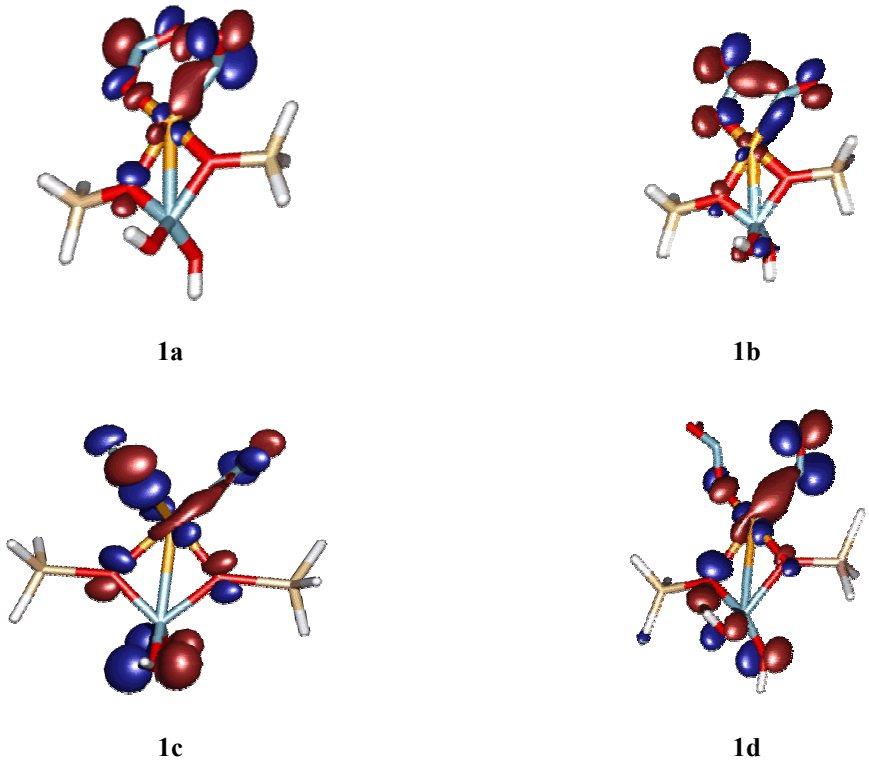

1a **1b**

1c **1d**

Figure 3.5 Representative orbitals of the NO-(NO_2)CuZ interaction in (NO_2)(NO)CuZ singlet species

The second most stable singlet **1b** lies 2.1 kcal/mol above **1a** and the bonding between NO and (NO_2)CuZ is similar to that discussed for **1a**. However, the orbital presented in Figure 3.5 shows that there is also a significant bonding interaction between both nitrogen atoms.

Structures **1c** and **1d** show a similar NO-(NO_2)CuZ bonding. Differences with respect to the previous **1a** and **1b** structures arise from the relative orientation of the NO_2 and NO ligands, which does not allow a stabilizing interaction between them. This interaction between ligands might be one of the reasons of the larger stability of **1a** and **1b**. In **1c**, NO_2 is nearly perpendicular to the Cu coordination plane. The Cu-O_3 (2.581 Å) distance seems to indicate that there is a weak interaction between these two atoms. This might explain the relative stabilities of **1c** and **1d**.

Three structures corresponding to (N_2O_3)CuZ complexes have been found (Figure 3.6). The triplet **3e** arises from the interaction of ON-NO_2 to CuZ in a bidentate manner through one oxygen of NO_2 and the oxygen of NO. It is worth noting that in this structure the N-N distance (1.436 Å) is significantly smaller than that obtained for free N_2O_3 (1.875Å). This can be understood considering the nature of the bonding of **3e**. Natural population analysis of **3e** indicates that the spin density on N_2O_3 is 1.17. Moreover, net atomic charges show that there is an important charge transfer (0.68) from CuZ to N_2O_3. Considering that the N_2O_3 ligand lies on the xz plane, one of the open shell orbitals corresponds to an antibonding combination between the d_{xz} orbital of the metal and the in plane lone pairs of the two interacting oxygens. The other open shell orbital mainly corresponds to a π orbital of N_2O_3, which has a bonding combination between the two nitrogen atoms, which accounts for the short N-N bond distance in this species. Thus, the bonding in **3e** can be better viewed as the interaction of $N_2O_3^-$ with CuZ^+. Structure **3e** lies 6.9 kcal/mol above the most stable **3a**.

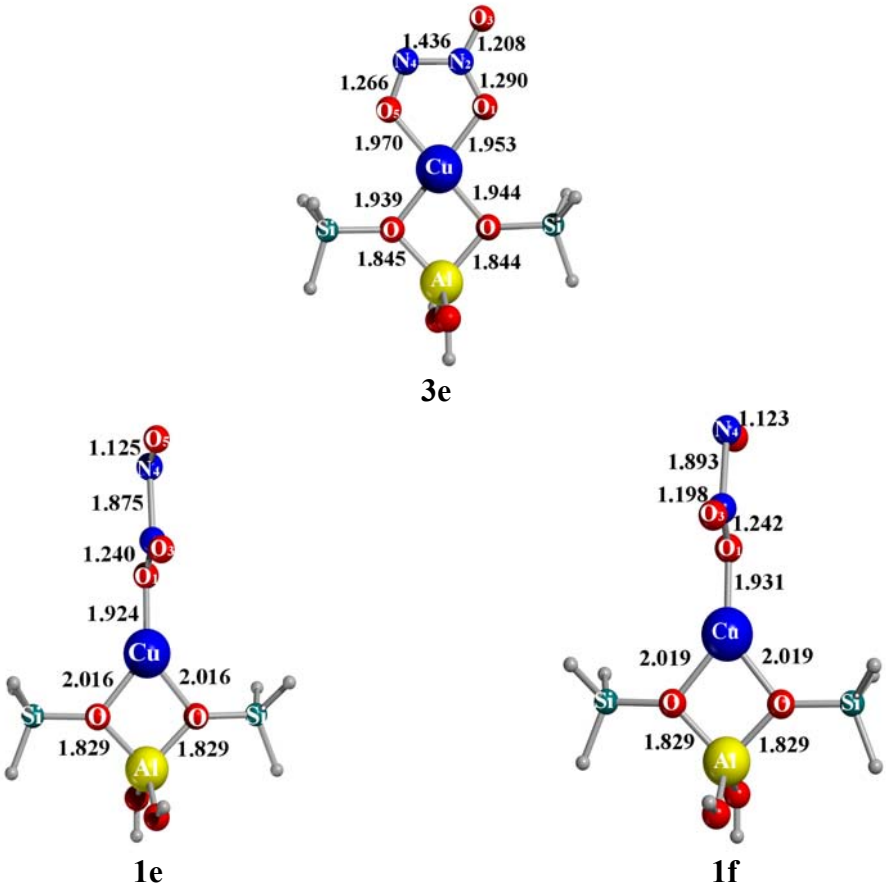

Figure 3.6 Optimised N_2O_3-CuZ triplet and singlet structures. Distance in Å , angles in degrees

A recent theoretical study on the potential energy surface of $N_2O_3^-$ has localised two energy minima corresponding to $[O_2N\text{-}NO]^-$.[65] The most stable one has a N-N distance of 2.22 Å, whereas the other one is only 3.5 kcal/mol higher in energy and presents a N-N distance of 1.56 Å. However, the potential energy surface of free $[O_2N\text{-}NO]^-$ in the 1.5-1.6 Å region, was found to be very flat. Our calculations seem to indicate that the interaction with CuZ stabilizes the structure with a short N-N distance.

The two (N_2O_3)CuZ singlet structures (**1f** and **1e**) correspond to a η^1-O coordination of N_2O_3 to CuZ. The binding energies are 24.9 kcal/mol for **1e** and 23.8 kcal/mol for **1f**. These are two different conformers arising from the rotation around the N-N bond. The N_2O_3-CuZ interaction is mainly electrostatic with a little charge transfer from Cu to N_2O_3. For this reason, the geometry of N_2O_3 ligand is very close to that of free N_2O_3[66] and thus, the N-N distance is considerably long. It must be mentioned that we could not find any (N_2O_3)CuZ singlet structure with an in-plane η^2-O,O coordination of N_2O_3 to CuZ, similar to **3e**. Any attempt to optimise such a specie evolved to a $(NO_2)(NO)$CuZ structure similar to **1b** but with the NO interacting through the oxygen atom.

Frequency calculations have been performed for all $(NO_2)(NO)$CuZ and (N_2O_3)CuZ structures. Table 3.3 presents the values corresponding to the N-O stretching modes of NO_2 and NO ligands. For comparison we have included those of isolated NO_2, NO_2^-, NO and N_2O_3. For $(NO_2)(NO)$CuZ species, in general, the stretching values associated with the NO_2 fragment are different from those we obtained for free NO_2 and NO_2^- due to the loss of symmetry. However, their values agree with a certain NO_2^- character. This is especially clear in **3a**, which has a η^2-O,O coordination mode and its frequencies are closer to those of NO_2^- than to those of NO_2. The ν_2 stretching frequency of NO_2, when acting as a monodentate ligand, ranges between 1466 and 1653 cm^{-1}. Experimental values assigned to NO_2 coordinated to CuZSM-5 are 1400-1500 and 1619-1630 cm^{-1}.[18,19,22]

Table 3.3 N-O and N-N stretching Frequencies (IR intensities) in $(NO_2)(NO)CuZ$ and $(N_2O_3)CuZ$ complexes. Frequencies in cm^{-1} (intensities in km/mol)

	NO_2		NO	
Structure	ν_1	ν_2	ν_3	ν_{NN}
3a	1203(325)	1334(20)	1986(61)	
3b	1106(308)	1474(402)	1897(307)	
3c	1012(201)	1653(430)	1897(276)	
3d	829(190)	1644(876)	1989(69)	
3e	1107(257)	1565(412)	1314(164)	801(5)
1a	1121(171)	1466(210)	1884(854)	
1b	1110(116)	1646(500)	1871(851)	
1c	1056(167)	1493(284)	1913(925)	
1d	880(540)	1628(305)	1935(845)	
1e	1273(27)	1609(299)	1955(1754)	822(11)
1f	1255(12)	1613(393)	1963(1479)	821(15)
N_2O_3	1369(301)	1693(414)	1937(453)	823(15)
NO_2	1386(0)	1679(433)		
NO_2^-	1268(507)	1346(23)		
NO			1971(42)	

The computed NO stretching mode lies in the 1870-1990 cm^{-1} range, in good agreement with the experimental values observed for NO-Cu^{2+}Z species (1880-1985 cm^{-1}).[18,19,22] In **3a** and **3d** where NO is weakly interacting with Cu, the determined values are very similar to that of free NO (1971 cm^{-1}). Furthermore, **3b** and **3c** present a less energetic NO mode, which is in good agreement with the elongation of the NO bond.

The NO stretching for the $(NO_2)(NO)CuZ$ singlet state structures is, in general, smaller than the one corresponding to isolated NO. This seems to be in contradiction with the shortening of the N_4-O_5 distance. However, this effect is also found in isolated N_2O_3 where the N_4-O_5 distance is shorter than the bond length in NO and the vibrational mode is also smaller. Despite that, within **1a** and **1d** structures there is a correlation between the N-O distance and the stretching frequency.

Finally stretching frequencies for (N_2O_3)CuZ singlet species (**1e** and **1f**) are very similar to those of free N_2O_3 and agree well with experimental assignment,[22] whereas for **3e** the stretching frequencies of N_2O_3 are quite different from those of **1e** and **1f**, especially for ν_3 associated to the NO fragment. This fact could be explained by the different coordination and nature of the N_2O_3-CuZ interaction. Despite the different N-N distance between singlet and triplet structures, the stretching N-N frequency is quite similar in both spin states.

The main goal of the study is to discuss if mechanism C can explain the catalytic activity of CuZSM-5. $(NO_2)(NO)$CuZ and (N_2O_3)CuZ species have been postulated as important intermediates of this mechanism. Consequently, the analysis of the stability of these species with respect to the catalytic species (O)CuZ (^{3}A) and 2NO ($^2\Pi$) is essential. The formation of all $(NO_2)(NO)$CuZ and (N_2O_3)CuZ species is highly exothermic (ΔH_{298} between –54.9 and –42.3 kcal/mol) and although the entropic effects disfavours their formation at room temperatures they are still thermodynamically favourable (ΔG_{298} between –35.6 and –22.9 kca/mol). Consequently, one might expect that (O)CuZ in a nitric oxide atmosphere and at low temperatures will evolve to (NO_2)CuZ and $(NO)(NO_2)$CuZ quite easily. This is in agreement with experimental studies which observe the formation of these species at room temperature.[4,6,18,19,22]

3.4.2 $(NO_2)(NO)$CuZ/(N_2O_3)CuZ decomposition

Starting from many of the previous described singlet and triplet structures, several attempts to find transition states that directly connect $(NO_2)(NO)$CuZ or (N_2O_3)CuZ to products have been done. However, we have not been able to find any transition state structure for the direct decomposition. This is not surprising since the direct decomposition from $(NO_2)(NO)$CuZ or (N_2O_3)CuZ to O_2 + N_2+ (O)CuZ requires an important electronic reorganization. That is, several multiple bonds have to be broken while other ones must be formed. Moreover, O_2 and (O)CuZ species present a triplet ground state. Thus, the conversion of $(NO_2)(NO)$CuZ or (N_2O_3)CuZ singlet state species to products might involve a crossing of singlet and triplet potential energy surfaces. The existence of a crossing point between singlet and triplet potential surfaces have been studied for free N_2O_3 and the obtained results indicated that the process might not be

through an intersystem crossing. All these unsuccessful attempts lead us to explore a multiple step mechanism involving other structures such (ONNOO)CuZ, (N_2O)CuZ, (O_2)CuZ and (N_2O)(O_2)CuZ species.

We will first describe these species and then the transition state structures that connect them. For each species, the optimised geometry structure will be presented as well as the L-CuZ interaction energy, the natural population analysis and the ligand stretching frequencies.

3.4.2.1 (ONNOO)CuZ species

ONNOO is a high energetic isomer of N_2O_3 which might be produced by an oxygen transfer from NO_2 to the oxygen of NO. This ONNOO isomer can coordinate to CuZ leading to different precursors of the formation of (N_2O)(O_2)CuZ from which O_2 and N_2 could easily be eliminated. Although many different coordinations of OONNO to CuZ could be considered, we have only studied those species arising from the transfer of one oxygen of NO_2 to NO in species **3e** and **1e**. One triplet (**3g**) and one singlet (**1g**) structures of (ONNOO)CuZ have been found to be minima of the respective potential energy surfaces and they are presented in Figure 3.7. Table 3.4 shows the (ONNOO)CuZ interaction energy, natural population analysis and ONNOO stretching frequencies.

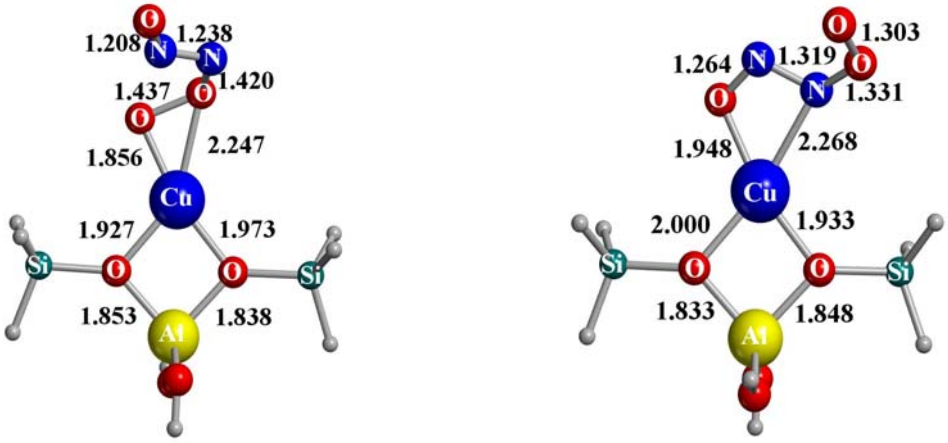

3g **1g**

Figure 3.7 Optimised (ONNOO)CuZ singlet and triplet structures. Distances in Å.

Table3.4 Interaction energies (in kcal/mol), natural population analysis and ligands stretching freqeuncies (in cm^{-1}) of (ONNOO)CuZ species.

		Charge			Spin			Frequencies			
Struct	ΔE^b	Z	Cu	L[a]	Z	Cu	L[a]	ν_{NO}	ν_{NO}	ν_{OO}	ν_{NN}
1g	–28.1	–0.75	1.15	–0.40				1364(30)	1061(63)	1061(304)	952(213)
3g	–50.6	–0.77	1.33	–0.56	0.13	0.55	1.32	1605(242)	827(77)	854(47)	1296(4)

[a] L stands for ONNOO ligand
[b] Relative energy with respect to ONNOO + CuZ asymptote

Both for the triplet **3g** and singlet **1g**, natural population analysis indicate that there is an important charge transfer from CuZ to the OONNO ligand. **1g** ONNOO-CuZ interaction is mainly electrostatic while for **3g** charge and spin analysis indicate that the bonding mainly arises from the interaction of the doublet spin state of $[OONNO]^-$ with the doublet CuZ^+. Again, due to the different nature of the bonding and the different modes of coordination (η^2-O,O or η^2-N,O) in the two spin states, the computed stretching frequencies in **1g** and **3g** show important differences (see Table 3.4). The observed variations, however, agree in general with the geometrical differences; that is, the shorter the distance the larger the stretching frequencies. Both for the singlet and triplet states, these species lie much higher in energy than the corresponding **1e**,**3e** structures. In the singlet state, the energy difference between **1e** and **1g** is 76.0 kcal/mol, whereas in the triplet state the **3e-3g** energy difference is 57.3 kcal/mol. This is not surprising considering that the energy difference between O_2NNO and OONNO isomers is 79.2 kcal/mol for the neutral and 51.1 kcal/mol for the anionic system.

3.4.2.2 $(N_2O)(O_2)$CuZ, (N_2O)CuZ and (O_2)CuZ species

As mentioned, $(N_2O)(O_2)$CuZ may be considered an intermediate of N_2 and O_2 elimination. Therefore, we have analysed different structures of this species both in the singlet and triplet state. In order to understand the nature of the bonding we have also analysed the interaction of each ligand with the zeolite; that is, the (N_2O)CuZ and (O_2)CuZ complexes.

The ground state of N_2O is a $^1\Sigma^+$ state. Since CuZ presents also a singlet ground state, the lowest energy state of $(N_2O)CuZ$ specie is expected to be a singlet. Despite that, we have also studied the triplet state. Figure 3.8 shows the optimised structures of the three localised minima: two singlets (**1h, 1i**) and one triplet (**3h**). Table 3.5 presents the interaction energies, natural population analysis and N_2O stretching frequencies of these species.

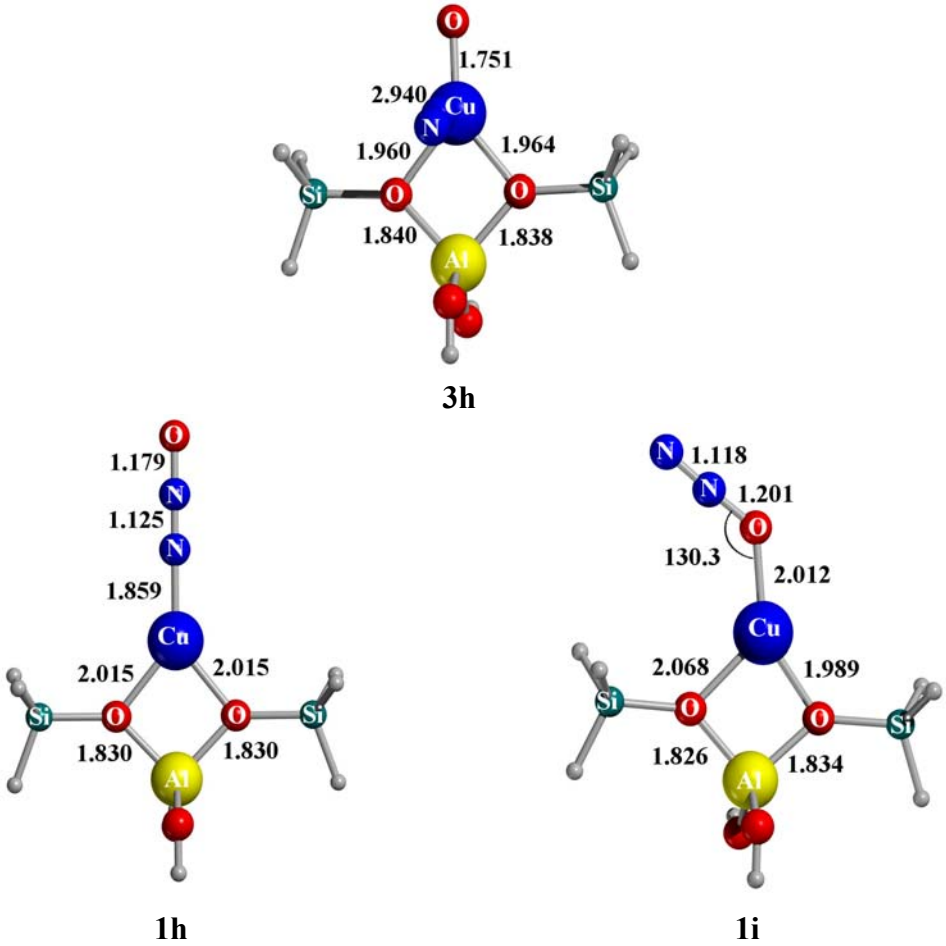

Figure 3.8 Optimised $(N_2O)CuZ$ singlet and triplet structures, distances in Å and angles in degrees

Structures **1h** and **1i** correspond to the interaction of N_2O through the N or through the O atoms, respectively. In both cases, population analysis shows that the bonding is mainly electrostatic. Thus, the geometry and stretching frequencies of the ligand in the complex differ only slightly from those of free N_2O.[67] The most important

variation corresponds to the N-O distance in the O-coordinated isomer (**1i**) which increases 0.016 Å and to the N-O stretching frequency that shows a red shift of 62 cm^{-1}. However, whereas in the N-coordinated structure (**1h**) the ligand interacts linearly with the metal, in the O-coordinated one (**1i**) the ligand adopts an angular orientation, with a NOCu angle of about 130^0. This can be understood considering that the metal cation seeks the most electron-rich region of the basic atom, which can be attributed to the lone pair of electrons. In the case of nitrogen, the lone pair lies on the intermolecular axis, whereas this is not the case for the oxygen atom.

Table 3.5 Interaction energy (in kcal/mol), natural population analysis and N_2O stretching frequencies (in cm^{-1}) of $(N_2O)CuZ$ singlet and triplet species.

			Charge			Frequencies	
	ΔE^b	Z	Cu	N_2O	N_2	ν_{NO}	ν_{NN}
3h	–20.4	–0.81	1.29	-0.49^{α}	0.01		2462(50)
1h	–24.8	–0.90	0.97	–0.07		1339(329)	2391(298)
1i	–13.1	–0.90	0.91	–0.01		1264(64)	2350(474)
N_2O						1326(68)	2345(386)

[a] Charge over O atom.
[b] Relative energies with respect to N_2O ($^1\Sigma_g^+$) + CuZ asymptote.

Experimental studies of N_2O adsorbed to CuZSM-5 provide values of 2230-2240 cm^{-1} for the N-N stretching, in good agreement with the results obtained in the present thesis (Table 3.5).[9,16,18,22]

Results indicate that the most stable structure is the N-coordinated one (**1h**), the (ONN)-CuZ binding energy being 24.8 kcal/mol. Structure **1i** lies 11.7 kcal/mol above **1h**. The preference for the N-coordination can be understood considering the larger polarizability of the nitrogen atom compared to that of the oxygen one, which results in a larger cation affinity. With respect to the triplet state, it can be observed in Figure 3.8 that the optimised structure does not correspond to $(N_2O)CuZ$ but to a $(N_2)(O)CuZ$ species (**3e**), in which N_2 is weakly interacting (1.7 kcal/mol) with (O)CuZ. The cleavage of the N-O bond is due to the fact that in the triplet state, one of the unpaired electrons

occupies a molecular orbital with and antibonding N-O character. This structure lies 4.5 kcal/mol above the lowest energy singlet one **1h**.

Figure 3.9 shows the optimised (O_2)CuZ structures and Table 3.6 presents the interaction energy, natural population analysis and vibrational frequencies of these same species. The optimisation of (O_2)CuZ, both in the triplet (**3j**) and singlet states (**1j**), show that the preferred interaction of O_2 to CuZ is side-on with the O_2 lying in the plane formed by Cu and the two oxygen atoms of the zeolite coordinated to Cu. In both cases, the O-O distance in the complex is significantly larger than that of free O_2.[68] Moreover, natural population analysis indicates that there is an important charge transfer from CuZ to the ligand. Therefore, O_2 acquires an important O_2^- superoxid character and because of that the O-O distance and stretching frequency resemble more to those of O_2^- than to those of neutral O_2. This is especially significant in the singlet state (**1j**) in which more charge transfer from CuZ to O_2 is observed and so, the O-O distance (1.342 Å) and O-O stretching frequency (1128 cm^{-1}) are very similar to those of free O_2^- (1.358 Å and 1155 cm^{-1}). The higher charge transfer in the singlet state and the smaller Cu-O distance indicate that the $O_2(^1\Sigma_u^+)$-CuZ interaction is stronger. However, the lowest energy structure corresponds to the triplet **3j** due to the high $^3\Sigma_g^- \rightarrow {}^1\Sigma_u^+$ transition energy (38.7 kcal/mol). The O_2-CuZ binding energy is 25.7 kcal/mol for **3j**. The singlet structure (**1j**) lies 12.8 kcal/mol above.

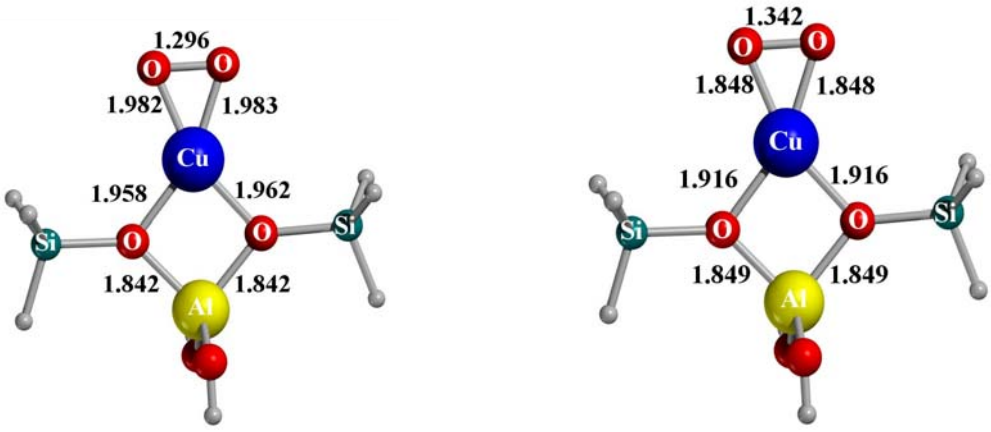

3j **1j**

Figure 3.9 Optimised (O_2)CuZ structure in the triplet (**3j**) and singlet (**1j**) states. Distances in Å.

Table 3.6 Interaction energies (in kcal/mol), natural population analysis and vibrational frequencies (cm^{-1}) of $(O_2)CuZ$ species.

		Charge			Spin			Freq.
Struc	ΔE^a	Z	Cu	O_2	Z	Cu	O_2	ν_{OO}
3j	–25.7	–0.81	1.24	–0.43	0.10	0.41	1.49	1234(126)
1j	–12.9	–0.71	1.30	–0.59				1128(176)
$O_2(^3\Sigma_g^-)$								1618(0)
$O_2^-(^2\Pi)$								1155(0)

[a] Relative energies with respect to $O_2(^3\Sigma_g^-)$ + CuZ

Let us now consider the $(N_2O)(O_2)CuZ$ species, with both ligands interacting with the zeolite. As for the precedent systems we have considered both the singlet and triplet states. Among all the structures explored, three triplet (**3k-3m**) and four singlet (**1k-1n**) structures have been localised on the respective potential energy surfaces (Figure 3.10). Table 3.7 presents the interaction energy of both ligands with respect to $CuZ + N_2O + O_2$ ground state, natural population analysis and vibrational frequencies. Although most of the starting geometries had the two ligands in the same Cu-Z coordination plane, most of them evolved to geometries in which one of the ligands (mainly N_2O) moved to the apical position. In contrast to what was found for $(N_2O)CuZ$ where N_2O interacts with CuZ in the CuZ plane, in this case the preferred coordination of N_2O to CuZ is through the O atom and not through N, as it was found in the $(N_2O)CuZ$ species. This is due to the fact that metal-N_2O repulsion is larger at the apical position than in the CuZ coordination plane. However, given the large metal-ligand distance at this position the N_2O-$(O_2)CuZ$ interaction energy is very small as well as the energy difference between the two possible coordinations (N or O).

Regarding the O_2 ligand, calculations show that, as for the $(O_2)CuZ$, the preferred coordination is the side-on one, both in the triplet and singlet states. Population analysis shows that the nature of the O_2-$(N_2O)CuZ$ bonding is very similar to that observed for $(O_2)CuZ$, in the absence of N_2O. This is not surprising considering that in **1k** and **3k** N_2O is far from the O_2CuZ plane and is very weakly bound and so it does not perturb the interaction of CuZ with O_2. It is also worth noting that monodentate coordinations (**1l-**

1n, **3m**) of O_2 to the metal are less favourable than the bidentate ones (**1k**,**3k**). Such coordinations show a smaller charge transfer from the metal to O_2, which leads to a weaker interaction energy.

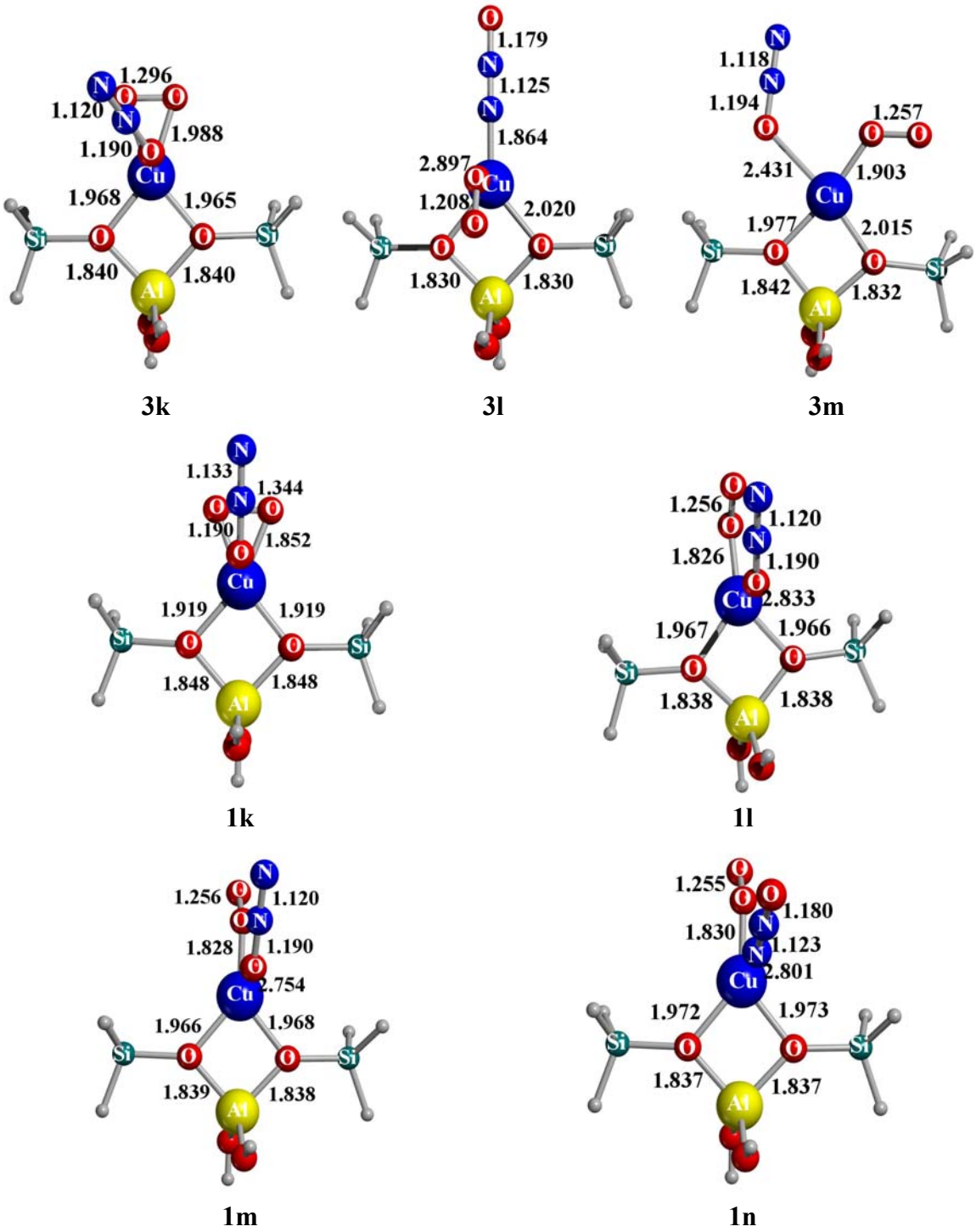

Figure 3.10 Optimised $(N_2O)(O_2)$CuZ singlet and triplet structures, distances in Å.

Table 3.7 Interaction energies (in kcal/mol), natural population analysis and vibrational frequencies (cm^{-1}) of $(N_2O)(O_2)CuZ$ species.

		Charge				Spin				Frequencies		
Struct.	ΔE^a	Z	Cu	N_2O	O_2	Z	Cu	N_2O	O_2	ν_{NN}	ν_{NO}	ν_{OO}
3k	–27.7	–0.88	1.25	0.07	–0.44	0.10	0.42	0.00	1.48	2352(425)	1313(97)	1235(170)
3l	–26.0	–0.90	0.97	–0.07	0.00	0.00	0.01	0.00	1.99	2391(313)	1338(337)	1615(2)
3m	–22.2	–0.83	1.17	0.00	–0.34	0.07	0.37	0.01	1.55	2357(373)	1294(47)	1308(510)
1k	–15.7	–0.71	1.32	0.00	–0.61					2356(388)	1312(96)	1125(120)
1l	–1.0	–0.79	1.16	0.00	–0.37					2354(389)	1312(96)	1354(343)
1m	–0.6	–0.79	1.16	0.00	–0.37					2352(416)	1311(92)	1354(326)
1n	–0.5	–0.80	1.15	0.01	–0.36					2357(524)	1343(67)	1358(339)
N_2O										2345(386)	1326(67)	
O_2												1618(0)

[a] Relative energies with respect to N_2O ($^1\Sigma^+$) + O_2 ($^3\Sigma_g^-$)+ CuZ asymptote.

Structure **3l** presents the N_2O ligand in the zeolite plane while O_2 is at the apical position and presents a long Cu-O_2 distance. In this case, the O_2-N_2OCuZ interaction is very weak and the N_2O-CuZ interaction is essentially equal to that described for structure **1h** ((ONN)CuZ).

It can be observed in Table 3.7 that all triplet structures are more stable than the singlet ones, the lowest energy one (**3k**) corresponding to a square pyramidal five coordination around the metal with N_2O at the apical position. As expected, due to the weak metal-N_2O interaction, the energy difference between the lowest singlet (**1k**) and the lowest triplet (**3k**) structures (12.1 kcal/mol) is very similar to that found between the singlet and triplet states of $(O_2)CuZ$ (12.8 kcal/mol).

Thermodynamic properties of all the species that might be involved in mechanism C with respect to the reactant 2NO + (O)CuZ asymptote are given in Table 3.8.

Table 3.8 Energies and thermodynamic parameters relative to the ground state (O)CuZ + 2NO asymptote.

Struct.		ΔE^a	$\Delta U_{0K}{}^a$	$\Delta H_{298K}{}^a$	$\Delta S_{298K}{}^b$	$\Delta G_{298K}{}^a$
1a	$ZCu(NO_2)(NO)$	–57.0	–52.8	–54.0	–78.7	–30.5
1b	$ZCu(NO_2)(NO)$	–54.9	–50.5	–51.7	–76.9	–28.8
1c	$ZCu(NO_2)(NO)$	–54.3	–50.3	–51.5	–73.1	–29.7
1d	$ZCu(NO_2)(NO)$	–49.1	–45.2	–46.4	–75.9	–23.8
1e	$ZCu(N_2O_3)$	–46.8	–42.2	–43.4	–68.8	–22.9
1f	$ZCu(N_2O_3)$	–45.6	–41.1	–42.3	–64.3	–23.3
1g	ZCu(ONNOO)	+29.2	+32.7	+31.5	–74.9	+53.8
1h	$ZCu(N_2O) + O_2$	–49.5	–46.5	–47.1	–34.0	–37.0
1i	$ZCu(N_2O) + O_2$	–37.8	–35.6	–36.2	–36.3	–25.4
1j	$ZCu(O_2) + N_2O$	–37.5	– 34.4	– 35.0	– 44.6	–21.7
1k	$ZCu(N_2O)(O_2)$	–40.3	–36.1	–36.7	–66.5	–16.4
1l	$ZCu(N_2O)(O_2)$	–25.6	–21.0	–22.2	–59.4	–4.5
1m	$ZCu(N_2O)(O_2)$	–25.2	–20.7	–21.9	–59.5	–4.2
1n	$ZCu(N_2O)(O_2)$	–25.1	–20.5	–21.7	–56.6	–4.9
3a	$ZCu(NO_2)(NO)$	–57.7	–53.7	–54.9	–64.7	–35.6
3b	$ZCu(NO_2)(NO)$	–52.1	–48.1	–49.3	–72.7	–27.6
3c	$ZCu(NO_2)(NO)$	–47.4	–43.4	–44.6	–70.9	–23.4
3d	$ZCu(NO_2)(NO)$	–45.7	–42.2	–43.4	–59.7	–25.6
3e	$ZCu(N_2O_3)$	–50.8	–46.2	–47.4	–82.2	–22.9
3g	ZCu(ONNOO)	+6.5	+10.0	+8.8	–72.5	+30.4
3h	$ZCuO(N_2) + O_2$	–45.0	–43.3	–43.9	–21.8	–37.4
3j	$ZCu(O_2) + N_2O$	–50.3	–47.5	–48.1	–38.7	–36.6
3k	$ZCu(N_2O)(O_2)$	–52.3	–48.0	–49.1	–58.0	–31.9
3l	$ZCu(N_2O)(O_2)$	–50.6	– 46.1	–47.3	–50.1	–32.3
3m	$ZCu(N_2O)(O_2)$	–46.7	–43.1	–44.2	–69.9	–23.4

[a] in kcal/mol

[b] in cal/(mol·K)

First of all, it can be observed that the formation of $(NO_2)(NO)CuZ$ from CuZ and two NO molecules is a very exothermic process. However, most of the exothermicity arises from the formation of $(NO_2)CuZ$ from (O)CuZ + NO, since the addition of a second NO molecule to $(NO_2)CuZ$ to form $(NO_2)(NO)CuZ$ has a reaction enthalpy at 298 K of only –0.5 kcal/mol for the singlet (**1a**) and –0.8 kcal/mol for the triplet (**3a**). $(N_2O_3)CuZ$ structures (**1e** and **3e**) lie 10.2 and 6.9 kcal/mol above **1a** and **3a**, respectively. Moreover, $(N_2O)CuZ + O_2$, $(O_2)CuZ + N_2O$ and $(N_2O)(O_2)CuZ$ are also more stable than reactants. Consequently, all the above reported structures, except those containing the high energetic ONNOO isomer, are energetically more stable than (O)CuZ (^3A) + 2 NO ($^2\Pi$). Although the entropic effect is destabilizing, at room temperature all the considered species, except **1g** and **3g**, are more stable than reactants, so that they might be formed during the decomposition process. However, their formation during the decomposition of NO can only be discussed after localising the transition state structures connecting them. In the following section the decomposition of $(NO_2)(NO)CuZ$ and $(N_2O_3)CuZ$ is discussed.

3.4.2.3 Transition state structures

The exploration of the potential energy surface to localise a multi-step decomposition mechanism has led to one triplet and one singlet decomposition paths involving (ONNOO)CuZ species. Figure 3.11 presents the singlet and triplet transition state structures which connect $(N_2O_3)CuZ$ with (ONNOO)CuZ species.

These transition state structures (**TS3e→3g** and **TS1e→1g**) are geometrically closer to **g** structures, as expected for very endothermic processes. This can be observed in **TS3e→3g** by the long N-O distance of the original NO_2 and also in the relative orientation of the ligand with respect the O-Cu-O plane. On the other hand, in **TS1e→1g** this is observed by the considerably short O-O and N-N distances especially compared to those of **1e**. Energetically, both for the singlet and triplet states, the energy barrier for this **e → g** isomerization reaction is very high: 74.5 kcal/mol for the triplet and 83.3 kcal/mol for the singlet state. On the other hand, at high temperatures these intermediates would be greatly destabilized due to the fact that their formation is not entropically favourable. For example, at 298 K the Gibbs energy of formation of **3e** is -22.9 kcal/mol, whereas at

the reaction temperature of 773K this value is +10.1 kcal/mol. Thus, such (N_2O_3)CuZ or $(NO_2)(NO)$CuZ species do not appear to be the key catalytic intermediates for NO decomposition.

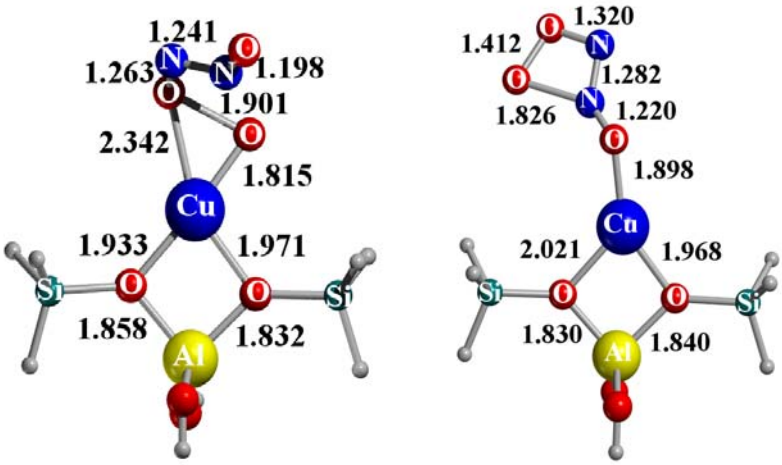

TS(3e→3g) **TS(1e→1g)**

Figure 3.11 Transition state structures connecting (N_2O_3)CuZ with (ONNOO)CuZ species. Distances in Å

Figure 3.12 presents the triplet transition state structure of the decomposition of **3g**. The transition state connecting (ONNOO)CuZ and $(N_2O)(O_2)$CuZ species has only been considered for the triplet state, given that our calculations indicate that the more favourable pathway occurs in the triplet potential energy surface.

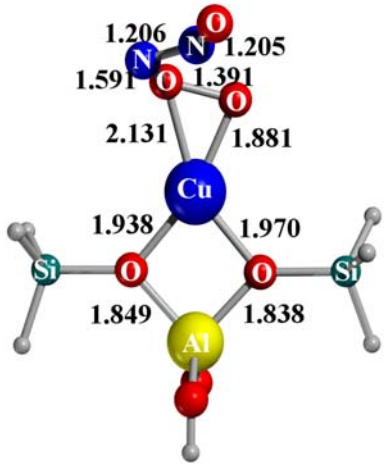

TS(3g→3k)

Figure 3.12 Transition state structure of **3g** decomposition. Distances in Å

Once the **3g** structure is formed, calculations show that it can easily evolve to $(N_2O)(O_2)CuZ$ species. **TS(3g→3k)** lies only 1.5 kcal/mol above (ONNOO)CuZ (**3g**). As mentioned, in **3k** N_2O is weakly bound and thus, at high temperatures (ONNOO)CuZ would evolve to $(O_2)CuZ + N_2O$. Figures 3.13 and 3.14 schematically represent the reaction energy profile for singlet and triplet potential energy surfaces. Formation of N_2 can be produced through the interaction of N_2O with CuZ after desorption of O_2 from $(O_2)CuZ$. However, given that the spin multiplicity of $(N_2O)CuZ$ corresponds to a singlet state and that of (O)CuZ to a triplet state, the unimolecular $(N_2O)CuZ \rightarrow (O)CuZ + N_2$ fragmentation involves the crossing of two potential energy surfaces. Alternatively, N_2 could be formed from the interaction of N_2O with (O)CuZ sites, through a (NNOO)CuZ transition state, which previous theoretical calculations have shown to have an energy barrier of about 36 kcal/mol.[40,41] In order to analyse the efficiency of the $(N_2O)CuZ \rightarrow N_2 + (O)CuZ$ process compared to this one, the following section presents the spin forbidden N_2O decomposition in Cu^+ZSM5

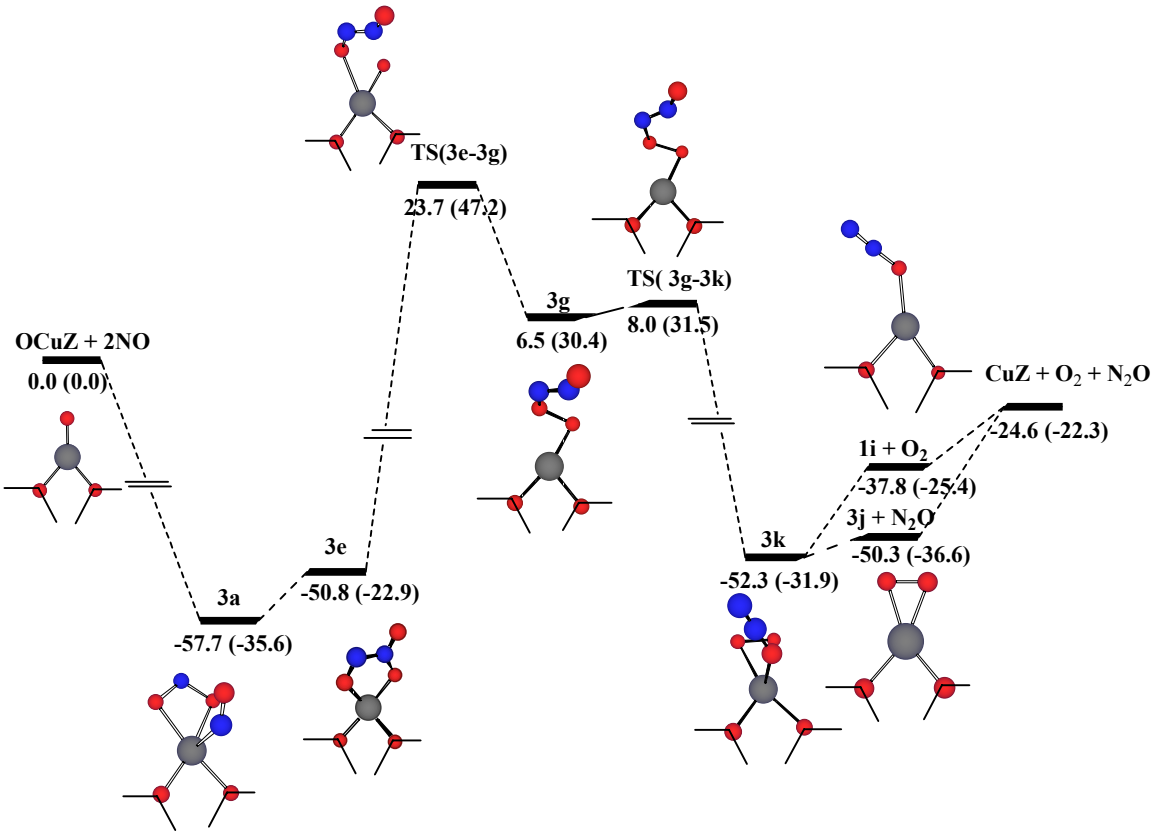

Figure 3.13 Schematic representation of the potential energy surface associated with the NO decomposition in the triplet state. Relative energies (ΔG^{o}_{298}) in kcal/mol

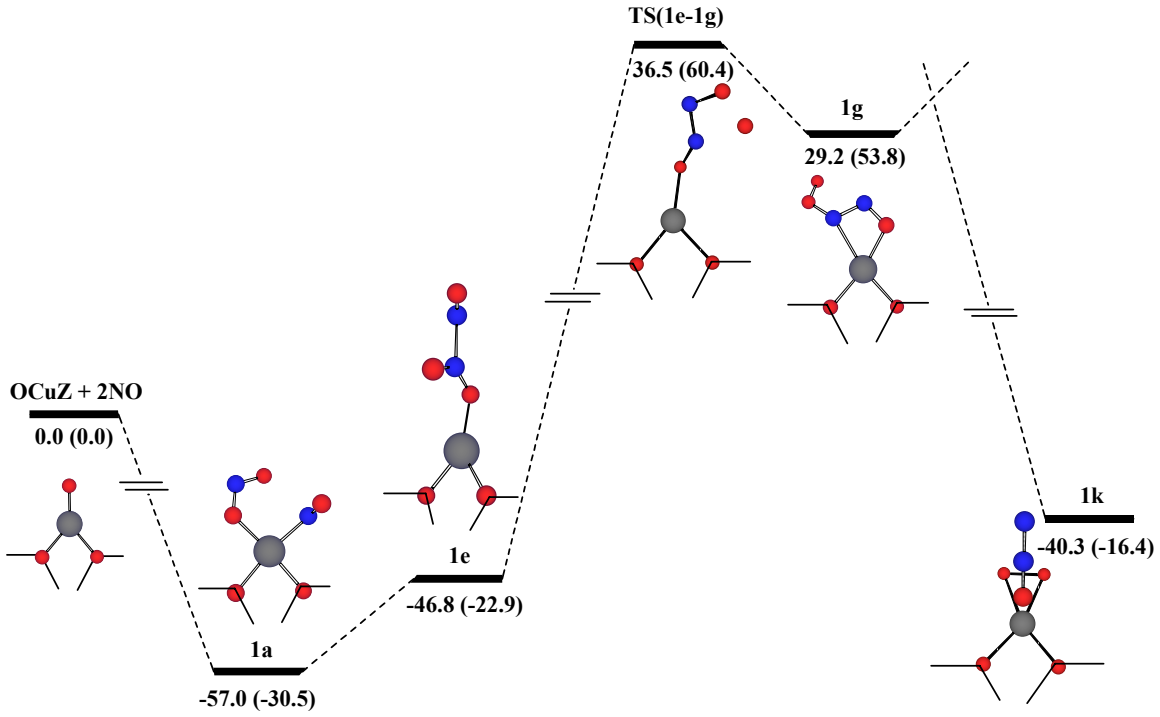

Figure 3.14 Schematic representation of the potential energy surface associated with the NO decomposition in the singlet state. Relative energies (ΔG^{o}_{298}) in kcal/mol

3.4.2.4 Spin forbidden N_2O decomposition in CuZSM-5.

As previously mentioned, N_2O can coordinate to CuZ through two different isomers: η^1-N and η^1-O. However, nitrogen elimination can only be produced from the N_2O-CuZ isomer. (N_2O)CuZ has a singlet ground state, whereas the ground state of (O)CuZ is a triplet. So, nitrogen elimination from (N_2O)CuZ is spin forbidden and has to take place through a crossing between singlet and triplet potential energy surfaces. The gas phase dissociation of N_2O ($^1\Sigma^+$) into N_2 ($^1\Sigma_g^+$) and O (^{3}P) is also spin forbidden.

To accurately study a spin-forbidden reaction, which involves a crossing of states with different multiplicities, a multireference approach must be used. Unfortunately, these methods are too computational demanding to be applied in our zeolite model. For this reason, we have performed B3LYP and CASSCF optimisations of N_2O and $[Cu–ON_2]^+$ systems to localise both reactant and product species. The crossing point of the spin forbidden dissociation has been computed using CASSCF level of theory and the

methodology implemented in GAUSSIAN package. In contrast, for $(N_2O)CuZ$ only B3LYP optimisations have been performed and the crossing point has been estimated.

Figure 3.15 presents a schematic orbital correlation diagram for the dissociation of N_2O into N_2 and O. A minimum active space for locating the singlet-triplet crossing point should include 4 electrons in 3 orbitals (2π and 8σ for N_2O). However, to get a consistent description of the reactant and the region of surface crossing is necessary to include the 3π orbitals. These active space is still not enough since in the region of surface crossing the 2π orbitals, which are mainly 2p(O), prefer to correlate with 3p(O) than with $1\pi_g(N_2)$. To prevent this, the 1π orbitals of N_2O have to be included in the active space. For these reasons, we have considered an active space of 8 electrons in 7 orbitals in the location of the crossing point. This active space includes the occupied 1π and 2π and the unoccupied 3π and 8σ of N_2O.

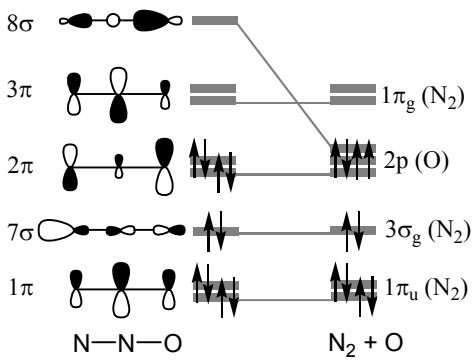

Figure 3.15 Schematic orbital correlation diagram for the dissociation of N_2O into N_2 and O.

For the ground state of $[Cu\text{-}ON_2]^+$ the interaction between Cu^+ and N_2O is mainly electrostatic, so that the orbitals of the N_2O fragment do not significantly change due to complexation. For the reaction products the oxygen 2p orbitals correspond to the antibonding 9σ and 4π orbitals of CuO^+. As a consequence, the orbital correlation diagram shown in Figure 3.15 may still be valid. However, when small active spaces are chosen for CASSCF calculations, the Cu d orbitals have a tendency to enter into the active space instead of some of the orbitals necessary to describe the singlet-triplet crossing. In spite of that, for the ground state of $Cu^+\text{-}ON_2$ we have been able to optimise

the geometry with an active space of 6 electrons in 6 orbitals. These are the occupied $3d_z^2$ and virtual $4d_z^2$ orbitals of Cu and the 2π and 3π orbitals of N_2O.

Figure 3.16 shows the structures of N_2O, and $[Cu\text{-}ON_2]^+$. N_2O is a linear molecule with a singlet ground state ($^1\Sigma^+$). The B3LYP geometry is closer to the experimental results than the CASSCF one.[69] For the $[Cu\text{-}ON_2]^+$ complex the N_2O ligand remains linear with a bent coordination to Cu^+. The B3LYP results are similar to those reported by Delabie and Pierloot.[70]

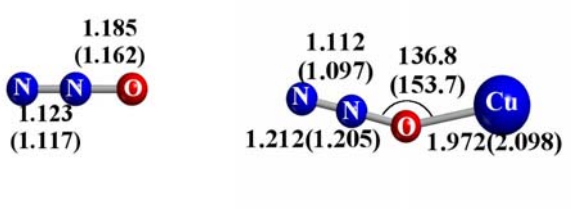

a **b**

Figure 3.16 Geometries of N_2O (a) and $[Cu\text{-}ON_2]^+$ (b) structures optimised at the B3LYP (CASSCF) level of theory. Bond lengths in Å angles in degrees.

We have localised the singlet-triplet crossing point for the gas phase N_2O dissociation at the CASSCF(8,7) level of calculation and its structure is presented in Figure 3.17a. The comparison with the ground state reactant (Figure. 3.16a) shows that the linear structure is conserved and that there is a remarkable lengthening of the O-N distance, whereas the N-N bond only slightly shortens. This result shows that the N-O distance is the most important geometry parameter for this process, in good agreement with the results previously reported.[71,72]

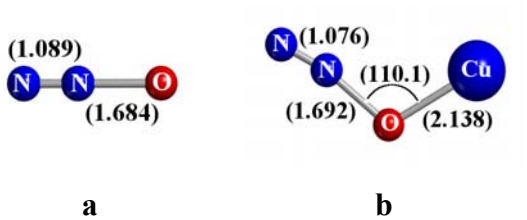

a **b**

Figure 3.17 Minimum energy singlet-triplet crossing points corresponding to the N-O dissociation of N_2O (a) and $Cu^+\text{-}ON_2$ (b) obtained at the CASSCF level of calculation. Bond lengths in Å, angles in degrees

The location of the singlet-triplet crossing point for $[Cu\text{-}ON_2]^+$ presents problems related to the selection of the active space. After several attempts, we have been able to localise such a crossing point with a (6,6) active space that includes the orbitals necessary to describe the singlet-triplet crossing. The structure of this crossing point is presented in Figure 3.17b and the corresponding active orbitals are shown in Figure 3.18. ψ_1 and ψ_5 are, respectively, the out of plane π and π^* of the N_2 fragment; ψ_2, ψ_3, and ψ_4 are mainly the O 2p orbitals that must be in the active space. Finally, ψ_6 has contributions from oxygen 3s and 3p and from Cu 4s and 4p. For the singlet state the first three orbitals are doubly occupied and for the triplet state the monooccupied orbitals are ψ_3 and ψ_4.

We can observe that the arrangement of the N_2O ligand at the crossing point is nearly linear and that the N-O and N-N distances are similar to the ones corresponding to the N_2O crossing point (Figure 3.17a). The value of the Cu-O bond length slightly increases, whereas there is an important decreasing of the Cu-O-N bond angle with respect to the ground state minimum shown in Figure 3.16b.

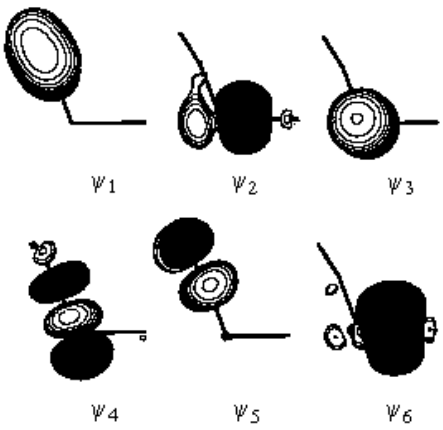

Figure 3.18 Active orbitals in the CASSCF(6,6) singlet-triplet crossing point of $Cu^+\text{-}ON_2$

The nature of the active orbitals is different from that corresponding to the ground state $[Cu\text{-}ON_2]^+$. For this reason, the energy difference between the crossing point and $[Cu\text{-}ON_2]^+$ cannot be calculated at the CASSCF(6,6) level of calculation. We have enlarged the active space up to CASSCF(20,14) to include the 3d orbitals of Cu and the $3\sigma_g$ and the in plane π and π^* orbitals of the N_2 fragment. With this active space we

have computed the energy difference between the $[Cu\text{-}ON_2]^+$ ground state minimum and the singlet-triplet crossing point.

Table 3.9 presents the energy values of the crossing point relative to the ground state reactant computed for N_2O and $[Cu\text{-}ON_2]^+$. In addition to the CASSCF results, we have calculated this energy difference at the B3LYP and CCSD(T)[73] levels of calculation.

For N_2O the CASSCF(8,7) energy is more than 10 kcal mol^{-1} lower than the CCSD(T) result. When the active space is enlarged to include the 7σ orbital of N_2O in a single point CASSCF(10,8) calculation, the energy notably increases. This result is due to the 7σ/8σ correlation in the ground state of N_2O. The inclusion of more dynamic correlation would approach the result to the CCSD(T) one. On the other hand, the B3LYP calculations overestimate the energy of the crossing point with respect to the CCSD(T) result. Values reported in the literature based on extensive MRCI calculations, in the 58-60 kcal mol^{-1} range, are very similar to our B3LYP result.[71,72]

Table 3.9. Energy[a] necessary to reach the singlet-triplet crossing points located at the CASSCF level of calculation

	N_2O[b]	$[Cu\text{-}ON_2]^+$[c]
CASSCF	43.4(49.3)[d]	(53.6)[e]
CCSD(T)	53.4	46.1
B3LYP	59.8	46.0

[a] in kcal mol^{-1}
[b] Geometries obtained at the CASSCF(8,7) level of calculation
[c] Geometries obtained at the CASSCF(6,6) level of calculation
[d] CASSCF(10,8) energy
[e] CASSCF (20,14) energy

For $[Cu\text{-}ON_2]^+$ B3LYP and CCSD(T) lead to almost the same result, whereas the CASSCF energy is more than 7 kcal mol^{-1} larger. Thus, considering that CASSCF calculations do not introduce enough dynamical correlation, it is observed that the

coordination of N_2O to Cu^+ produce a decrease of the energy necessary to reach the singlet-triplet crossing point.

For $(N_2O)CuZ$ the size of the system precludes the location of the crossing point. Based on the observation that for the other two systems the main geometry parameter for such a process is the N-O distance, we have calculated the energies of the singlet and triplet states at different values of the N-O distance allowing the relaxation of the remaining geometry parameters. To verify that this approach leads to a reasonable approximation to the real crossing point, we have done the same kind of calculation for N_2O and $[Cu\text{-}ON_2]^+$. The results obtained are summarized in Table 3.10.

Table 3.10. N-O distances[a] and energies[b] of the estimated singlet-triplet crossing points computed at the B3LYP level of calculation

	N-O	ΔE(S/T)
N_2O	1.72	64
$[Cu\text{-}ON_2]^+$	1.75	46
$(N_2O)CuZ$	1.58	26

[a] in Å
[b] in kcal mol^{-1}

For N_2O the two energy profiles cross at a N-O distance slightly longer than the value corresponding to the real crossing point and the energy is about 5 kcal mol^{-1} higher. For $[Cu\text{-}ON_2]^+$ a similar behaviour is observed for the N-O distance, but the energy difference is the same as the one computed for the real crossing point. The N-O distance is shorter and the energy is lower than the results reported by Delabie and Pierloot.[70] These differences are understandable if one takes into account that in Delabie and Pierloot's study only the geometry of the singlet was allowed to relax and that the energy of the triplet was calculated from single point calculations. From the results obtained for N_2O and $[Cu\text{-}ON_2]^+$ we can conclude that the estimation of the crossing points from constrained optimisations on the singlet and triplet potential energy surfaces provides reasonable results.

Table 3.10 shows that for $(N_2O)CuZ$ the crossing between the singlet and triplet profiles appears earlier, at a N-O distance of 1.58 Å, and that the energy necessary to reach the crossing is notably smaller. Our results can be compared to those reported by Sengupta et al. (N-O= 1.89 Å and $\Delta E(S/T)$ = 23 kcal mol^{-1}).[32] We can observe that there is quite good agreement in the energy necessary to reach the crossing point, but that in our results the crossing point is closer to the ground state reactants. It should be noted that Sengupta et al. have used a small $Al(OH)_4$ cluster to model the zeolite and that their energies have been calculated at a lower level of calculation.

The results summarized in Table 3.10 show that complexation by Cu^+ or CuZ facilitates the intersystem crossing associated to the N-O dissociation by decreasing the energy necessary to reach the singlet-triplet crossing point. Figure 3.19 schematically presents the energetics associated to the N-O dissociation of N_2O in the gas phase and in the presence of Cu^+ and CuZ. The gas phase process is clearly endothermic. Complexation by Cu^+ or CuZ decreases the reaction energy for the N-O dissociation and for CuZ the process becomes exothermic.

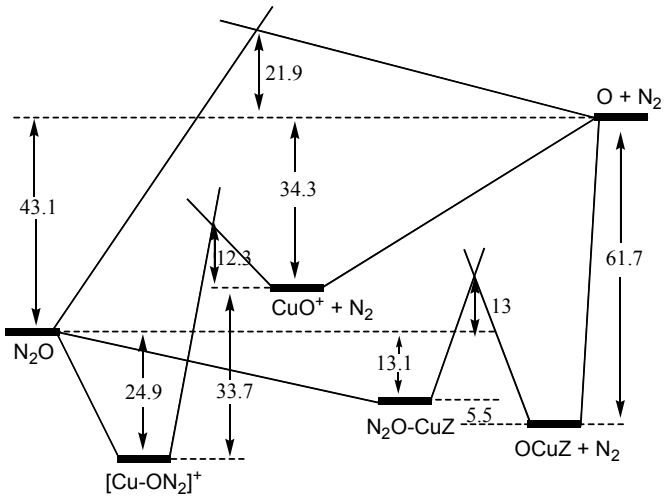

Figure 3.19 Schematic energy diagram for the N-O bond dissociation of N_2O in the gas phase and catalysed by Cu^+ and CuZ. Energies in kcal/mol

The comparison between the reaction energies shown in Figure 3.19 and the energies necessary to reach the singlet-triplet crossing point (Table 3.10) shows that there is a correlation between both magnitudes. The main factor in the diminution of the

reaction energy is the strength of the Cu-O bond in the reaction product. CuZ is a stronger catalyst than Cu^+, since the Cu-O bond has an important ionic $O^-Cu^{2+}Z^-$ contribution. On the other hand, the Cu-O bond of CuO^+ is weaker and has mainly a Cu^+O character. The natural population analysis shows that the charge on the oxygen atom is –0.50 for (O)CuZ and –0.14 for CuO^+.

These results clearly demonstrate the high catalytic activity of CuZ for the N_2O decomposition process. That is, as a consequence of the strength of the Cu-O bond in (O)CuZ, the singlet-triplet crossing point of (N_2O)CuZ lies only about 13 kcal mol^{-1} above the CuZ + N_2O asymptote, whereas for the gas phase process this energy is almost 60 kcal mol^{-1}. The energy to reach the crossing point is considerably smaller than the previously computed energy barrier for OCuZ + N_2O (36 kcal/mol). Thus, formation of N_2 would more probably occur through the interaction of N_2O with CuZ

3.5 Concluding remarks

The electronic structure of (NO_2)(NO)CuZ and (N_2O_3)CuZ, which have been postulated as intermediate species in the NO decomposition, have been studied using a T3 cluster and B3LYP level of theory. Several singlet and triplet state structures have been located as minima of the potential energy surface. All structures are more stable (~ 55 kcal/mol) than the (O)CuZ + 2 NO asymptote and their relative energies are within a range of 12 kcal mol^{-1}.

The most stable (NO_2)(NO)CuZ structure (**3a**) is a triplet state in which Cu has a square pyramidal five-coordination with NO in the apical position, the bonding interaction between (NO_2)CuZ and NO being mainly electrostatic. This structure is the only one that maintains a bidentate η^2-O,O coordination for NO_2. The lowest singlet (NO_2)(NO)CuZ structure (**1a**) lies only 0.7 kcal/mol above **3a**. Its geometry and bonding interaction differs substantially from **3a**, since in **1a** the coordination around Cu is square planar and the NO-(NO_2)CuZ interaction has a significant covalent contribution. (N_2O_3)CuZ structures are generally slightly less stable than (NO_2)(NO)CuZ ones. The (N_2O_3)-CuZ interaction also differs depending on the spin multiplicity, (N_2O_3)CuZ triplet

structure (**3e**) presents an important $(N_2O_3)^-$-CuZ^+ ionic behaviour, while the interaction in the singlet structures (**1e, 1f**) is mainly electrostatic.

Consequently, our calculations seem to indicate that at low temperatures and in the presence of an excess of nitric oxide, $(NO_2)(NO)CuZ$ or N_2O_3CuZ would be produced. However, energy barriers corresponding to their decomposition are very high. Therefore, $(NO_2)(NO)CuZ$ or $(N_2O_3)CuZ$ species cannot be considered as key intermediates of the NO decomposition. At high temperatures, the interaction of 2 NO molecules with (O)CuZ could evolve to $(O_2)CuZ + N_2O$ through a (ONNOO)CuZ like transition state, which lies 23.7 kcal/mol above the (O)CuZ + 2NO asymptote. The obtained results agree well with the experimental studies, which detect $(NO_2)(NO)CuZ$ and $(N_2O_3)CuZ$ complexes at low temperatures, whereas significant amounts of N_2 and O_2 only appear at high temperatures.[4,6,18,19,22]

Other authors have proposed that the reaction mechanism of NO decomposition takes place through mechanism B (see page 36).[34,40,41] The rate determinant step of this process, $(O)CuZ + N_2O \rightarrow CuZ + O_2 + N_2$, is reported to present an energy barrier of about 36 kcal/mol. This energy barrier is significantly larger than the relative energy (23.7 kcal/mol) of **TS(3e→3g)** with respect the (O)CuZ +2NO reactants. Therefore, at high temperatures, at which species $(NO_2)(NO)CuZ$ or $(N_2O_3)CuZ$ will not be formed and in a rich NO atmosphere, the interaction of two NO molecules with (O)CuZ to lead to $(O_2)CuZ$ appears to be a more favourable process than the one previously reported for the $(O)CuZ + N_2O$ reaction. It should be mentioned, however, that at high temperatures and due to entropic effects, both pathways will probably compete, the dynamical aspects being responsible of the resulting process.

The formation of N_2 can be reached from N_2O. From N_2O two different paths have been suggested for the decomposition to N_2. On one hand, the interaction of N_2O with (O)CuZ through the oxygen would evolve to $(O_2)CuZ + N_2$ through a $[NNOO\text{-}CuZ]^{\ddagger}$ transition state. As mentioned above this reaction presents and energy barrier of about 36 kcal/mol. On the other hand, $(N_2O)CuZ$ species could dissociate in N_2 + (O)CuZ. This dissociation is spin forbidden and presents the crossing point connecting $(N_2O)CuZ$ and N_2 + (O)CuZ at 26 kcal/mol above the $(N_2O)CuZ$ intermediate.

The study of the global problem, considering all variables, is so vast that it is not feasible in a thesis project. In particular, the present study does not consider several aspects such as other possible catalytic species, the role of the channel, the effect of temperature, etc. However, we expect that the analysis of the electronic structures of many possible intermediates, the computation of their vibrational frequencies, as well as the description of a possible decomposition path may help in the understanding of the NO decomposition by CuZSM-5.

References and notes

(1) Glebov, L. S.; Zakirova, A. G.; Tret'yakov, V. F.; Burdeinaya, T. N.; Akopova, G. S. *Pretroleum Chemistry* **2002**, *42*, 143.

(2) Wayne, R. P. *Chemistry of atmospheres*; Oxford University Press: New York, 1986.

(3) Seinfeld, J. H. *Atmospheric Chemistry and Physics of Air Pollution*; John Wiley and Sons: New York, 1986.

(4) Iwamoto, M.; Hamada, H. *Catal. Today* **1991**, *10*, 57.

(5) Tomašić, V.; Gomzi, Z.; Zrnčević, S. *Appl. Catal. B: Environmental* **1998**, *18*, 233.

(6) Centi, G.; Perathoner, S. *Appl. Catal. A: General* **1995**, *132*, 179.

(7) Shelef, M. *Chem. Rev.* **1995**, *95*, 209.

(8) Li, Y.; Hall, W. K. *J. Catal.* **1991**, *129*, 202.

(9) Ganemi, B.; Björnbom, E.; Paul, J. *Appl. Catal. B: Environmental* **1998**, *17*, 293.

(10) Beutel, T.; Sárkány, J.; Lei, G.-D.; Yan, J. Y.; Sachtler, W. M. H. *J. Phys. Chem.* **1996**, *100*, 845.

(11) Lo Jacono, M.; Fierro, G.; Dragone, R.; Feng, X.; d'Itri, J.; Hall, W. K. *J. Phys. Chem. B* **1997**, *101*, 1979.

(12) Lamberti, C.; Bordiga, S.; Salvalaggio, M.; Spoto, G.; Zecchina, A.; Geobaldo, F.; Vlaic, G.; Bellatreccia, M. *J. Phys. Chem. B* **1997**, *101*, 344.

(13) Turnes-Palomino, G.; Fisicaro, P.; Bordiga, S.; Zecchina, A.; Giamello, E.; Lamberti, C. *J. Phys. Chem. B* **2000**, *104*, 4064.

(14) Dědeček, J.; Wichterlová, B. *J. Phys. Chem.* **1994**, *98*, 5721.

(15) Larsen, S. C.; Aylor, A.; Bell, A. T.; Reimer, J. A. *J. Phys. Chem.* **1994**, *98*, 11533.

(16) Konduru, M. V.; Chuang, S. S. C. *J. Phys. Chem. B* **1999**, *103*, 5802.

(17) Grünert, W.; Hayes, N. W.; Joyner, R. W.; Shpiro, E. S.; Siddiqui, M. R. H.; Baeva, G. N. *J. Phys. Chem.* **1994**, *98*, 10832.

(18) Valyon, J.; Hall, W. K. *J. Phys. Chem.* **1993**, *97*, 1204.

(19) Spoto, G.; Zecchina, A.; Bordiga, S.; Ricchiardi, G.; Martra, G.; Leofanti, G.; Petrini, G. *Appl. Catal. B: Environmental* **1994**, *3*, 151.

(20) Dědeček, J.; Sobalík, Z.; Tvarůžková, Z.; Kaucký, D.; Wichterlová, B. *J. Phys. Chem.* **1995**, *99*, 16327.

(21) Wichterlová, B.; Dědeček, J.; Vondrová, A. *J. Phys. Chem.* **1995**, *99*, 1065.

(22) Aylor, A. W.; Larsen, S. C.; Reimer, J. A.; Bell, A. T. *J. Catal.* **1995**, *157*, 592.
(23) Spoto, G.; Bordiga, S.; Scarano, D.; Zecchina, A. *Catal. Lett.* **1992**, *13*, 39.
(24) Cheung, T.; Bhargava, S. K.; Hobday, M.; Foger, K. *J. Catal.* **1996**, *158*, 301.
(25) Schay, Z.; Knözinger, H.; Guczi, L.; Pál-Borbély, G. *Appl. Catal. B: Environmental* **1998**, *18*, 263.
(26) Giamello, E.; Murphy, D.; Magnacca, G.; Morterra, C.; Shioya, Y.; Nomura, T.; Anpo, M. *J. Catal.* **1992**, *136*, 510.
(27) Jang, H.-J.; Hall, W. K.; d'Itri, J. L. *J. Phys. Chem.* **1996**, *100*, 9416.
(28) Prestipino, C.; Berlier, G.; Llabrés-Xamena, F. X.; Spoto, G.; Bordiga, S.; Zecchina, A.; Turnes-Palomino, G.; Yamamoto, T.; Lamberti, C. *Chem. Phys. Lett.* **2002**, *363*, 389.
(29) Anpo, M.; Matsuoka, M.; Shioya, Y.; Yamashita, H.; Giamello, E.; Morterra, C.; Che, M.; Patterson, H. H.; Webber, S.; Ouellette, S.; Fox, M. A. *J. Phys. Chem.* **1994**, *98*, 5744.
(30) Dandekar, A.; Vannice, M. A. *Appl. Catal. B: Environmental* **1999**, *22*, 179.
(31) Pápai, I.; Goursot, A.; Fajula, F.; Plee, D.; Weber, J. *J. Phys. Chem.* **1995**, *99*, 12925.
(32) Sengupta, D.; Adams, J. B.; Schneider, W. F.; Hass, K. C. *Catal. Lett.* **2001**, *74*, 193.
(33) Sierraalta, A.; Añez, R.; Brussin, M.-R. *J. Catal.* **2002**, *205*, 107.
(34) Tajima, N.; Hashimoto, M.; Toyama, F.; El-Nahas, A. M.; Hirao, K. *Phys. Chem. Chem. Phys.* **1999**, *1*, 3823.
(35) Trout, B. L.; Chakraborty, A. K.; Bell, A. T. *J. Phys. Chem.* **1996**, *100*, 17582.
(36) Trout, B. L.; Chakraborty, A. K.; Bell, A. T. *J. Phys. Chem.* **1996**, *100*, 4173.
(37) Blint, R. J. *J. Phys. Chem.* **1996**, *100*, 19518.
(38) Goodman, B. R.; Schneider, W. F.; Hass, K. C.; Adams, J. B. *Catal. Lett.* **1998**, *56*, 183.
(39) Ramprasad, R.; Hass, K. C.; Schneider, W. F.; Adams, J. B. *J. Phys. Chem. B* **1997**, *101*, 6903.
(40) Schneider, W. F.; Hass, K. C.; Ramprasad, R.; Adams, J. B. *J. Phys. Chem. B* **1998**, *102*, 3692.
(41) Schneider, W. F.; Hass, K. C.; Ramprasad, R.; Adams, J. B. *J. Phys. Chem. B* **1997**, *101*, 4353.
(42) Yokomichi, Y.; Yamabe, T.; Ohtsuka, H.; Kakumoto, T. *J. Phys. Chem.* **1996**, *100*, 14424.

(43) Berthomieu, D.; Krishnamurty, S.; Coq, B.; Delahay, G.; Goursot, A. *J. Phys. Chem. B* **2001**, *105*, 1149.

(44) Šponer, J. E.; Sobalík, Z.; Leszczynski, J.; Wichterlová, B. *J. Phys. Chem. B* **2001**, *105*, 8285.

(45) Delabie, A.; Pierloot, K.; Groothaert, M. H.; Schoonheydt, R. A.; Vanquickenborne, L. G. *Eur. J. Inorg. Chem.* **2002**, 515.

(46) Delabie, A.; Pierloot, K.; Groothaert, M. H.; Weckhuysen, B. M.; Schoonheydt, R. A. *Micropor. and Mesopor. Mater.* **2000**, *37*, 209.

(47) Delabie, A.; Pierloot, K.; Groothaert, M. H.; Weckhuysen, B. M.; Schoonheydt, R. A. *Phys. Chem. Chem. Phys.* **2002**, *4*, 134.

(48) Pierloot, K.; Delabie, A.; Groothaert, M. H.; Schoonheydt, R. A. *Phys. Chem. Chem. Phys.* **2001**, *3*, 2174.

(49) Treesukol, P.; Limtrakul, J.; Truong, T. N. *J. Phys. Chem. B* **2001**, *105*, 2421.

(50) Nachtigall, P.; Nachtigallová, D.; Sauer, J. *J. Phys. Chem. B* **2000**, *104*, 1738.

(51) Nachtigallová, D.; Nachtigall, P.; Sierka, M.; Sauer, J. *Phys. Chem. Chem. Phys.* **1999**, *1*, 2019.

(52) Rodríguez-Santiago, L.; Sierka, M.; Branchadell, V.; Sodupe, M.; Sauer, J. *J. Am. Chem. Soc.* **1998**, *120*, 1545.

(53) Sierka, M.; Sauer, J. *J. Chem. Phys.* **2000**, *112*, 6983.

(54) Eichler, U.; Kölmel, C. M.; Sauer, J. *J. Comput. Chem.* **1996**, *18*, 463.

(55) Becke, A. D. *J. Chem. Phys.* **1993**, *98*, 5648.

(56) Lee, C.; Yang, W.; Parr, R. G. *Phys. Rev. B* **1988**, *37*, 785.

(57) Schäfer, A.; Horn, H.; Ahlrichs, R. *J. Chem. Phys.* **1992**, *97*.

(58) Reed, A. E.; Curtiss, L. A.; Weinhold, F. *Chem. Rev.* **1988**, *88*, 899.

(59) Frisch, M. J.; Trucks, G. W.; Schlegel, H. B.; Gill, P. M. W.; Johnson, B. G.; Robb, M. A.; Cheeseman, J. R.; Keith, T. A.; Petersson, G. A.; Montgomery, J. A.; Raghavachari, K.; Al-Laham, M. A.; Zakrzewski, V. G.; Ortiz, J. V.; Foresman, J. B.; Cioslowski, J.; Stefanov, B. B.; Nanayakkara, A.; Challacombe, M.; Peng, C. Y.; Ayala, P. Y.; Chen, W.; Wong, M. W.; Andres, J. L.; Replogle, E. S.; Gomperts, R.; Martin, R. L.; Fox, D. J.; Binkley, J. S.; Defrees, D. J.; Baker, J.; Stewart, J. P.; Head-Gordon, M.; Gonzalez, C.; Pople, J. A. Gaussian 94; Gaussian Inc.: Pittsburgh, 1995.

(60) Frisch, M. J.; Trucks, G. W.; Schlegel, H. B.; Scuseria, G. E.; Robb, M. A.; Cheeseman, J. R.; Zakrzewski, V. G.; Montgomery, J. A.; Stratmann, R. E.; Burant, J. C.; Dapprich, S.; Millam, J. M.; Daniels, A. D.; Kudin, K. N.; Strain,

M. C.; Farkas, O.; Tomasi, J.; Barone, V.; Cossi, M.; Cammi, R.; Mennucci, B.; Pomelli, C.; Adamo, C.; Clifford, S.; Ochterski, J.; Petersson, G. A.; Ayala, P. Y.; Cui, Q.; Morokuma, K.; Malick, D. K.; Rabuck, A. D.; Raghavachari, K.; Foresman, J. B.; Cioslowski, J.; Ortiz, J. V.; Baboul, A. G.; Stefanov, B. B.; Liu, G.; Liashenko, A.; Piskorz, P.; Komaromi, I.; Gomperts, R.; Martin, R. L.; Fox, D. J.; Keith, T.; Al-Laham, M. A.; Peng, C. Y.; Nanayakkara, A.; Gonzalez, C.; Challacombe, M.; Gill, P. M. W.; Johnson, B. G.; Chen, W.; Wong, M. W.; Andres, J. L.; Head-Gordon, M.; Replogle, E. S.; Pople, J. A. Gaussian 98; Gaussian Inc.: Pittsburgh, 1998.

(61) Roos, B. O. *Adv. Chem. Phys.* **1987**, *69*, 399.

(62) MOLPRO is a package of ab initio programs written by H.J. Werner and P. J. Knowles, with contributions from R. D. Amos, A. Bernhardsson, A. Berning, P. Celani, D. L. Cooper, M. J. O. Deegan, A. J. Dobbyn, F. Eckert, C. Hampel, G. Hetzer, T. Korona, R. Lindh, A. W. Lloyd, S. J. McNicholas, F. R. Manby, W. Meyer, M. E. Mura, A. Nicklass, P. Palmieri, R. Pitzer, G. Rauhut, M. Schütz, H. Stoll, A. J. Stone, R. Tarroni, and T. Thorsteinsson

(63) Rodríguez-Santiago, L.; Solans-Monfort, X.; Sodupe, M.; Branchadell, V. *Inorg. Chem.* **1998**, *37*, 4512.

(64) The optimized N-O distance is 1.148 Å

(65) Chen, M.; Zhou, M.; Qin, Q. *Chem. Phys. Lett.* **2000**, *321*, 498.

(66) The optimized geometry parameters of free N_2O_3 are O_1-N_2= 1.202 Å, N_2-O_3 = 1.201 Å, N_2-N_4 = 1.875 Å, N_2-O_5 = 1.133 Å, O_1-N_2-O_3 = 131.1, O_1-N_2-N_4= 112. 6, N_2-N_4-O_5 = 106.6

(67) The optimised distances are N-N= 1.123 Å and N-O= 1.185 Å

(68) The optimized O-O bond length is 1.209 Å

(69) Rayner-Canham, G. The Group 15 elements. In D*escriptive Inorganic Chemistry;* Rayner-Canham, G., Ed.; W. H. Freeman and Company: New York, 1997; pp 268.

(70) Delabie, A.; Pierloot, K. J. *Phys. Chem. A* 2**002,** 1*06,* 5679.

(71) Hwang, D.-Y.; Mebel, A. M. C*hem. Phys.* 2**000,** 2*59,* 89.

(72) Chang, A. H. H.; Yarkony, D. R. J. *Phys. Chem.* 1**993,** 9*9,* 6824.

(73) Raghavachari, K.; Trucks, G. W.; Pople, J. A.; Head-Gordon, M. C*hem. Phys. Lett.* 1**989,** 1*57,* 479.